STUDY EFFECT OF ULTRASONIC MELT TREATMENT ON MICROSTRUCTURE AND MECHANICAL PROPERTIES OF AN Al-Ce ALLOY

BY

62011098 MR. BHUVASU PANYADEE
62011150 MS. MANASNAN RAWANG
62011220 MR. PORNPONG RAICHAROEN

ADVISOR

ASST.PROF.DR. SUWAREE CHANKITMUNKONG

A PROJECT SUBMITTED IN PARTIAL FULFILLMENT OF THE REQUIREMENTS FOR THE DEGREE OF BACHELOR OF ENGINEERING IN INDUSTRIAL ENGINEERING AND LOGISTICS MANAGEMENT (INTERNATIONAL PROGRAM)
SCHOOL OF ENGINEERING

KING MONGKUT'S INSTITUTE OF TECHNOLOGY LADKRABANG

ACADEMIC YEAR 2022

FACULTY OF ENGINEERING

KING MONGKUT'S INSTITUTE OF TECHNOLOGY LADKRABANG

PROJECT CERTIFICATE

Thesis Title	STUDY EFFECT OF ULTRASONIC MELT TREATMENT ON MICROSTRUCTURE AND MECHANICAL PROPERTIES OF AN Al-Ce ALLOY
Student	Mr. Bhuvasu Panyadee Mr. Pornpong Raicharoen Ms. Masanan Rawang
Degree	Bachelor of Engineering in Industrial Engineering and Logistics Management King Mongkut's Institute of Technology Ladkrabang
Project advisor	Signed Suwaree (Asst. Prof. Dr. Suwaree Chankitmunkong)

Thesis Title	STUDY EFFECT OF ULTRASONIC MELT TREATMENT ON MICROSTRUCTURE AND MECHANICAL PROPERTIES OF AN Al-Ce ALLOY
Student	Mr. Bhuvasu Panyadee Mr. Pornpong Raicharoen Ms. Masanan Rawang
Degree	Bachelor of Engineering in Industrial Engineering and Logistics Management King Mongkut's Institute of Technology Ladkrabang
Academic Year	2022
Thesis Advisor	Asst. Prof. Dr. Suwaree Chankitmunkong

ABSTRACT

Aluminum-Cerium alloys are of research interest nowadays because of their potential benefits in industry sectors such as aerospace, marine applications, and automotive. This thesis aims to develop Aluminum-Cerium alloys by studying the various aspects of Aluminum-Cerium alloys that add Magnesium, Scandium, and Zirconium at different cooling rates to analyze the microstructure, hardness, and tensile properties. The study of the microstructure of alloys found that intermetallic and grain sizes are highly different between Al-15Ce and Al-15Ce-0.75Mg-0.2Sc-0.2Zr. Regarding the high cooling rate, Al-15Ce-0.75Mg-0.2Sc-0.2Zr have an average intermetallic size smaller than Al-15Ce at 46.11% and an average grain size at 88%, respectively. Regarding the low cooling rate, Al-15Ce-0.75Mg-0.2Sc-0.2Zr have an average intermetallic size smaller than Al-15Ce at 43.69% and average grain size at 91.42%, respectively. The addition of Sc and Zr in Al-15Ce-0.75Mg alloy formed the primary phase of Al_3(Sc, Zr), which can significantly increase the harness from 52.19 HB to 69.39 HB. In terms of mechanical properties, tensile strength increased from 34.65 MPa for Al-15Ce to 60.69 MPa for Al-15Ce-0.75Mg-0.2Sc-0.2Zr alloy with aging 350 °C. In conclusion, developing an aluminum cerium alloy by adding elements to enhance microstructure and improve mechanical qualities, including hardness and strength in adding Magnesium, Scandium, and Zirconium, positively affects the thesis. It hopes to be engaging in the industry.

ACKNOWLEDGEMENT

Thesis on the study effect of ultrasonic melt treatment on microstructure and mechanical properties of Aluminum-Cerium alloys as part of the Bachelor of Engineering Program, Department of Industrial Engineering, which can accomplish. We want to express our gratitude to those who have kindly provided knowledge, advice, examination, correction and advice on problems encountered during the dissertation process until this thesis can be completed well.

We want to thank Dr. Suwaree Chankitmankong, a lecturer of Department of Industrial Engineering lecturer at King Mongkut's Institute of Technology Ladkrabang who is an advisor who spends time to educate, give advice during operation until the completion of this thesis is entirely correct.

Thank you to the Faculty of Engineering at King Mongkut's University of Technology Thonburi for supporting their materials and equipments. In addition, the care during the work was safe during the operation until successful.

Thank you to the Department of Industrial Engineering at King Mongkut's Institute of Technology Ladkrabang, courtesy of the location, equipment, laboratory and staff who helped, including the operation cost of this thesis.

Finally, we would like to thank our parents and family for their support and encouragement as well as friends for giving advice and exchanging knowledge in preparing this thesis. The working group sincerely hopes that this thesis will benefit to the study of materials and contribute to the development of knowledge and ability in material engineering.

CONTENTS

LIST OF FIGURES

LIST OF TABLES

CHAPTER 1 INTRODUCTION

1.1 State of introduction

Aluminum is a highly versatile form and valuable metal in various industrial applications. Aluminum is vital in multiple industrial sectors, including aerospace, automotive, transportation, construction, electrical, packaging, and more. Its importance stems from its unique combination of properties, making it an essential material for numerous industries.

Cerium alloys are lightweight and have good thermal performance through surface engineering techniques; cerium serves various alloys that increase Aluminum's wear and corrosion resistance [1]. According to the study, Aluminum can be combined with cerium to produce a highly castable alloy compatible with conventional aluminum alloy additives and has significantly better high-temperature performance [2].

The grain refinement of aluminum alloy can be achieved by ultrasonic melt treatment. Alloys' structures can be changed using the liquid metal processing technique known as ultrasonic treatment (UST). Aluminum alloys are known to undergo grain refinement due to ultrasonic melt treatment (UST). The fundamental idea is introducing acoustic waves higher than 17 kHz into liquid metal. Oscillations with a high frequency and high amplitude cause the melt to cavitate and also encourage vigorous mixing [3].

Aging treatment is a heat treatment process that can be strengthened and improve their mechanical characteristics using the low-temperature heat treating technique known as age hardening, often referred to as precipitation hardening [4]. Intermetallic complexes harden and precipitate in large quantities during artificial aging. This precipitation enhances the mechanical properties [5].

Adding alloying elements in the aluminum alloy can improve the microstructure and mechanical properties; for example, adding mg in Al Ce alloy found that adding Mg will increase strengthening. Al-Ce-Mg cast alloys have demonstrated a considerable increase in hardness and outstanding thermal stability compared to binary Al- Ce alloys [6]. The addition of Zr and Sc offers enormous potential with improving creep-resistance, heat stability, and mechanical properties and decreases the grain size [7].

Therefore, this research focuses on studying the effect of ultrasonic melt treatment on the microstructure and mechanical properties of an Al-Ce alloy with Sc and Zr addition.

1.2 Objective

1. To study the microstructure of aluminum cerium alloy.
2. To study the mechanical properties of aluminum cerium alloy.
3. To study the effect of adding Mg, Sc, and Zr elements on microstructure and mechanical properties of aluminum cerium alloy.
4. To study the combined influence of ultrasonic treatment on the microstructure, and mechanical properties of aluminum cerium alloys.
5. To study the effect of aging on the mechanical properties of aluminum cerium by adding Sc and Zr.

1.3 Research Scope

1. This research study is on Al-15Ce and Al-15Ce-0.75Mg, and Al-15Ce-0.75Mg-0.2Sc-0.2Zr alloy.
2. This research uses ultrasonic treatment in casting process of aluminum alloy.
3. The grain refinement in the Al-Ce alloy was analyzed to examine its effects on various properties.
4. Tests were conducted to assess the mechanical properties and properties such as strength tests, and test hardness,
5. The influence of the microstructure on different properties was analyzed and discussed based on the experimental results.
6. The impact of aging on the microstructure and its effects on various properties were analyzed and discussed, considering the experimental data.

1.4 Expected benefits

1. The knowledge of experimental results can be applied to develop the aluminum alloy in the industry.
2. To learn about the properties of aluminum alloys in different grades and guidelines for developing new grades of cerium aluminum alloy to meet the needs of properties for industrial applications.
3. To understand the role of alloying element addition (Sc, Zr) in aluminum alloy for improving microstructure and mechanical properties through the aging process.
4. To learn about the process of improving the structure and properties of aluminum alloy by using the ultrasonic method.

1.5 Research schedule and detailed activity

This project has a period starting from August 2022 to May 2023 with details and an operating schedule as shown in Table.

Table 1 Action Plan

List	Aug	Sep	Oct	Nov	Dec	Jan	Feb	Mar
Search for interesting topic for this study	←	→						
Research for theories, material, equipment, working Process	←	—	—	→				
Planning and design for experiment			←	→				
Experiment				←	—	→		
Analysis					←	—	→	
Conclusion and suggest							↔	
Report and document								↔

CHAPTER 2 THEORIES AND LITERATURE REVIEW

2.1 Al-Ce alloys

Al-Ce alloys are alloys composed of aluminum (Al) and cerium (Ce) as the primary alloying elements. Adding cerium to aluminum forms a composite material that exhibits enhanced strength, improved heat resistance, and increased corrosion resistance compared to pure aluminum. These alloys find applications in aerospace, automotive, electronics, and construction industries, where their strength, heat, and corrosion resistance combination are valuable. In addition, Al-Ce alloys are lightweight, making them attractive for weight-sensitive applications, while the unique properties of cerium contribute to their overall performance. Al-Ce alloys' specific composition and properties can vary depending on the desired application and manufacturing processes [8, 9].

2.1.1 Properties of Al-Ce alloys

1. Strength: The addition of cerium to aluminum results in improved mechanical strength. Al-Ce alloys exhibit higher tensile strength, yield strength, and hardness than pure aluminum [8, 9].
2. Corrosion Resistance: Al-Ce alloys demonstrate enhanced corrosion resistance, including resistance to pitting, intergranular, and general corrosion. This property makes them suitable for applications in corrosive environments [8, 9].
3. High-Temperature Stability: Al-Ce alloys exhibit good thermal stability and can withstand high temperatures without significantly losing mechanical properties [8, 9, 10].
4. Lightweight: Aluminum is naturally lightweight, and adding cerium does not significantly increase the density of the alloy. Al-Ce alloys retain the advantageous lightweight characteristic of aluminum, making them desirable for weight-sensitive applications [9, 10].
5. Ductility: Al-Ce alloys maintain reasonable ductility levels, allowing for forming and shaping processes [9, 10].
6. Weldability: Al-Ce alloys generally exhibit good weldability, enabling efficient joining using various welding techniques [10].

2.2.2 Advantages and disadvantages of Al-Ce alloys

1. Improved Strength: Al-Ce alloys offer higher mechanical strength compared to pure aluminum [8, 9, 10].
2. Corrosion Resistance: The addition of cerium enhances the corrosion resistance of aluminum, making Al-Ce alloys suitable for use in corrosive environments [8, 9, 10].
3. High-Temperature Stability: Al-Ce alloys can withstand elevated temperatures without significant losing mechanical properties [8, 9]

4. Lightweight: Al-Ce alloys retain the lightweight nature of aluminum, providing weight advantages in various applications [9, 10].
5. Weldability: Al-Ce alloys can be efficiently joined using different welding techniques [9, 10].
6. Increased Strength: Al-Ce alloys exhibit improved mechanical strength, including tensile strength, yield strength, and hardness, compared to pure aluminum [8, 9].
7. Increased Strength: Al-Ce alloys exhibit improved mechanical strength, including tensile strength, yield strength, and hardness, compared to pure aluminum [10].
8. Limited Availability of Cerium: Cerium's limited availability may impact the scalability of using Al-Ce alloys in large-scale production [10].

2.2 Casting Process

During the casting manufacturing process, a liquefied substance, such as molten metal, is poured into the cavity of a specially-made mold and left solidified in the mold. After solidification, the workpiece is removed from the mold to either go through various finishing processes or be used as the finished product. Cast products are used in a variety of applications, such as automotive components, aerospace parts, etc., and are frequently produced using casting methods to produce intricate solid and hollow shapes [11].

2.3 Role of alloying element

2.3.1 Role of magnesium

Magnesium is a potent element in aluminum alloys. When Magnesium adding to an Al-Ce alloy, magnesium forms compounds with cerium, which promotes the formation of fine-grained microstructures. This refinement of the grain structure can improve the alloy's mechanical properties, such as strength and toughness. Magnesium addition can enhance the strength of Al-Ce alloys. The formation of magnesium-containing compounds strengthens the alloy and hinders the movement of dislocations, which are responsible for plastic deformation, as shown in **Figure 1** [12].

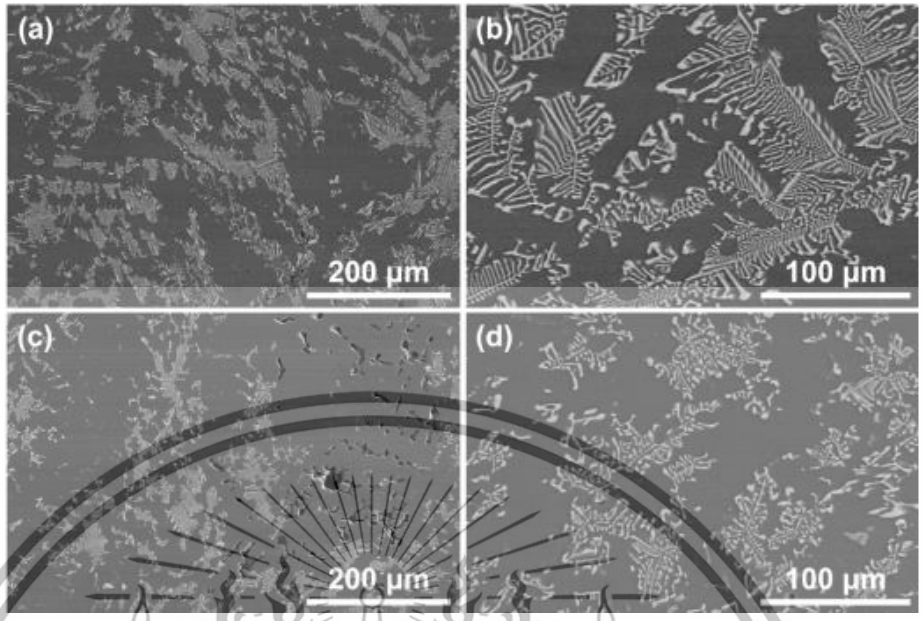

Figure 1 SEM of Al-6.9Ce-9.3Mg (wt.%), showing (a) representative microstructure of as-received alloy with α-Al (Mg) and eutectic Al (Mg)-$Al_{11}Ce_3$ regions, (b) detail of fine eutectic Al (Mg) $Al_{11}Ce_3$ with micron-scale eutectic structure, (c) casting porosity, and (d) after aging for eight weeks at 450 °C.

Magnesium is a smaller atom than aluminum, and when added to an Al-Ce alloy, it can occupy the interstitial spaces between aluminum atoms [13]. The presence of magnesium atoms makes it more difficult for them to move and increases the alloy's strength and hardness. Magnesium can also form precipitates in the Al-Ce alloy through heat treatment processes [13]. A supersaturated solid solution is formed when an Al-Ce alloy with magnesium is heated and rapidly quenched. Subsequent aging or heat treatment at a lower temperature allows the precipitation of fine and dispersed magnesium-containing compounds. These precipitates act as obstacles for dislocations, impeding their movement and strengthening the Al-Ce alloy [13].

In addition, the study focused on the microstructure stability and strengthening mechanisms of Al-Ce based alloys after heat treatment at different temperatures. the paper reports the effect of Mg, additions on the thermal stability of near eutectic Al-12Ce alloy [14].

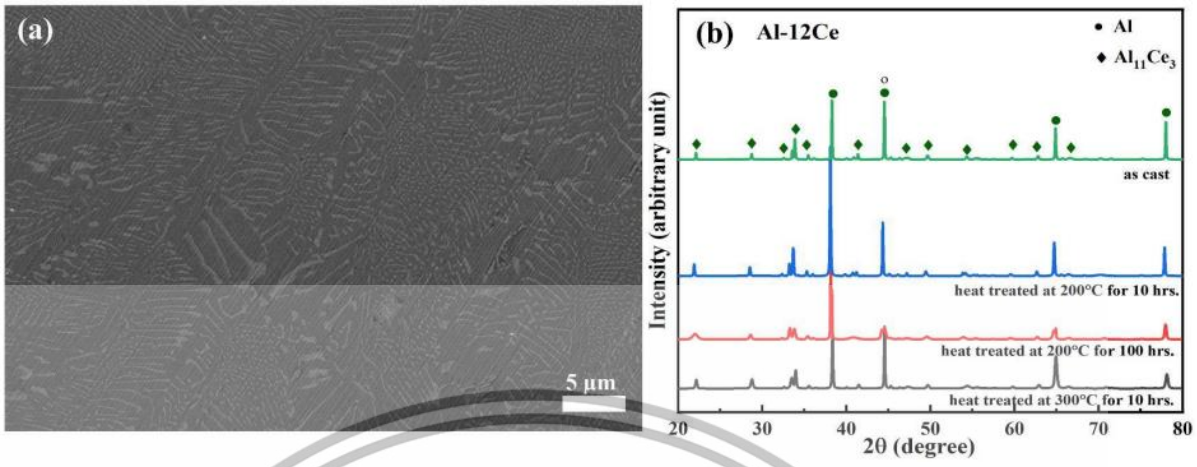

Figure 2 (a) FESEM micrograph of as-cast Al-12Ce (wt.%) alloy, (b) XRD pattern.

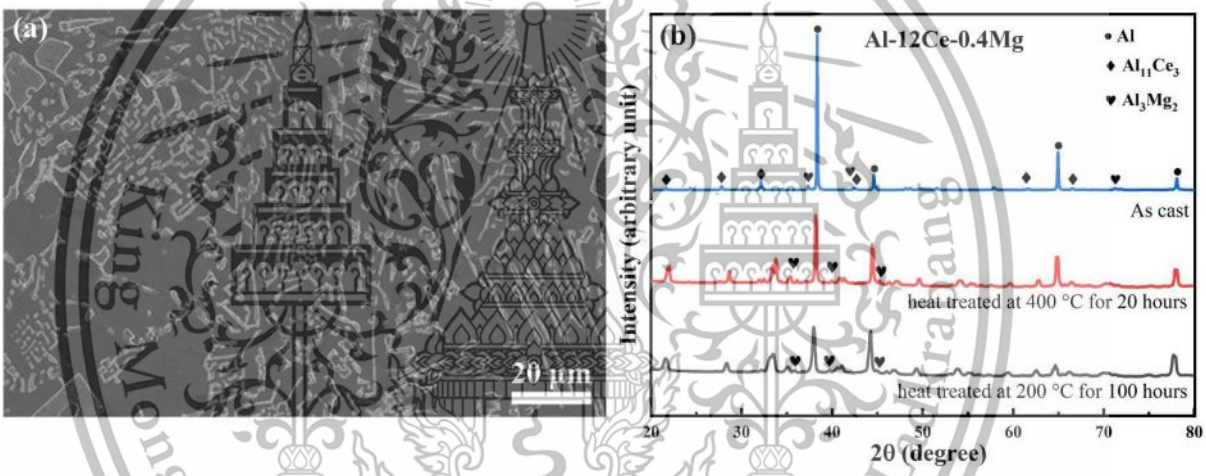

Figure 3 (a) FESEM micrograph of as-cast Al-12Ce-0.4Mg (wt.%) alloy, showing primary precipitation of intermetallic $Al_{11}Ce_3$, (b) XRD pattern.

Figure 2 and **Figure 3** show the XRD patterns of Al-12Ce alloy with different heat treatment conditions. Figure 2 shows the XRD pattern of the as-cast alloy, while Figure 3 shows the XRD pattern of the alloy heat-treated at 300°C for 10 hours. The XRD pattern of the as-cast alloy shows the presence of $Al_{11}Ce_3$ phases, while the XRD pattern of the heat-treated alloy shows the presence of $Al_{11}Ce_3$ and Al_3Mg_2 intermetallic phases. The intensity of the $Al_{11}Ce_3$ peaks decreases after heat treatment, while the intensity of the Al_3Mg_2 peak increases. This indicates that the heat treatment causes a transformation of the intermetallic phases in the alloy [14].

2.3.2 Role of scandium and zirconium

Scandium and Zirconium atoms can adsorb on the $Al_{11}Ce_3$ phase surfaces and control the growth process, as shown in **Figure 4 (b, e, h, k)**. Adding Sc and Zr can refine the size of primary $Al_{11}Ce_3$ phases and act as heterogeneous nucleation sites [15]. **Table 3** Sc and Zr atoms dissolved in the matrix as a decomposed solid solution precipitated the Al_3(Sc, Zr) phases after thermal exposure, which maintained full coherency with the Al matrix, leading to a hardness increase rather than a decrease [15].

Table 2 Measured compositions of the Al–15Ce (Sc-Zr) alloys (wt %).

Samples	Ce	Sc	Zr	Al
0Sc–0Zr	14.97	0	0	Bal.
0.13Sc–0.06Zr	15.21	0.13	0.06	Bal.
0.23Sc–0.10Zr	15.09	0.23	0.10	Bal.
0.49Sc–0.21Zr	15.02	0.49	0.21	Bal.

The paper explains that the study investigates the effect of Sc/Zr addition on the microstructure, mechanical properties, and thermal stability of hyper eutectic Al-Ce alloys. The study aims to understand the modification of Sc/Zr addition on Ce-rich phases and investigate the thermal stability of the alloy by the Al_3(Sc, Zr) precipitation hardening effect [15].

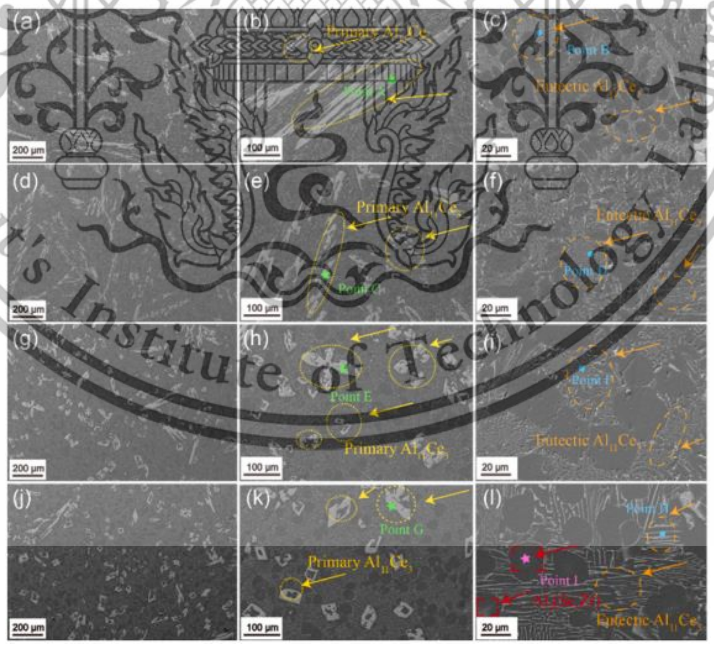

Figure 4 SEM images of Al–15Ce alloys with different Sc/Zr content: (a–c) 0Sc-0Zr; (d–f) 0.13Sc-0.06Zr; (g–i) 0.23Sc–0.10Zr; (j–l) 0.49Sc-0.21Zr.

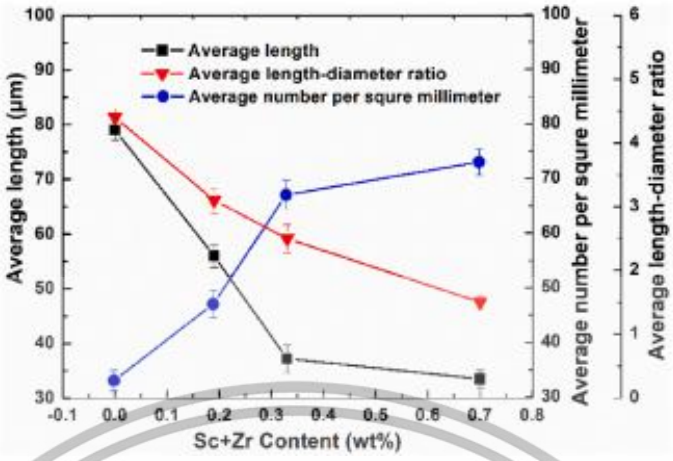

Figure 5 Evolution of the average length, length-diameter ratio, and number per square millimeter of primary $Al_{11}Ce_3$ phases in the Al–15Ce alloys with the coupling addition of Sc and Zr elements.

As shown in **Figure 5,** the size of primary $Al_{11}Ce_3$ phases were refined from ~79 μm to ~56 μm in the 0.13 wt.% Sc, 0.06 wt.% Zr addition alloy [15]. As the total Sc/Zr content increased, forming primary Al_3(Sc, Zr) phases could significantly refine the primary $Al_{11}Ce_3$ phases by acting as heterogeneous nucleation sites. Therefore, in 0.23 wt.% Sc, 0.16 wt.% Zr, and 0.49 wt.% Sc-0.23 wt.% Zr alloys, the modification effect on primary $Al_{11}Ce_3$ phases was based upon the interaction of adsorption effect and heterogeneous nucleation [15]. The sizes of primary $Al_{11}Ce_3$ phases were refined to ~37 μm and ~32 μm, leading to a significant improvement in ultimate tensile strength, yield strength, and elongation in the 0.49 wt.% Sc-0.23 wt.% Zr alloy compared to the unmodified alloy [15].

Table 3 Measured compositions of Al-5Ce (wt.%) alloys.

Alloy	Ce	Zr	Sc	Al
Al-5Ce	5.01	–	–	Bal.
Al-5Ce-0.2Zr	4.98	0.21	–	Bal.
Al-5Ce-0.2Sc	4.97	–	0.19	Bal.
Al-5Ce-0.2Zr-0.2Sc	5.08	0.18	0.23	Bal.

The introduction of the paper discusses the use of rare-earth elements, particularly cerium (Ce), in improving the properties of aluminum alloys. The Ce element has been explored for micro-alloying in aluminum and magnesium alloys to improve properties or modify second phases. The paper focuses on the micro-addition of Scandium and Zirconium in Al-5Ce alloys to improve their strength and decrease segregation [7].

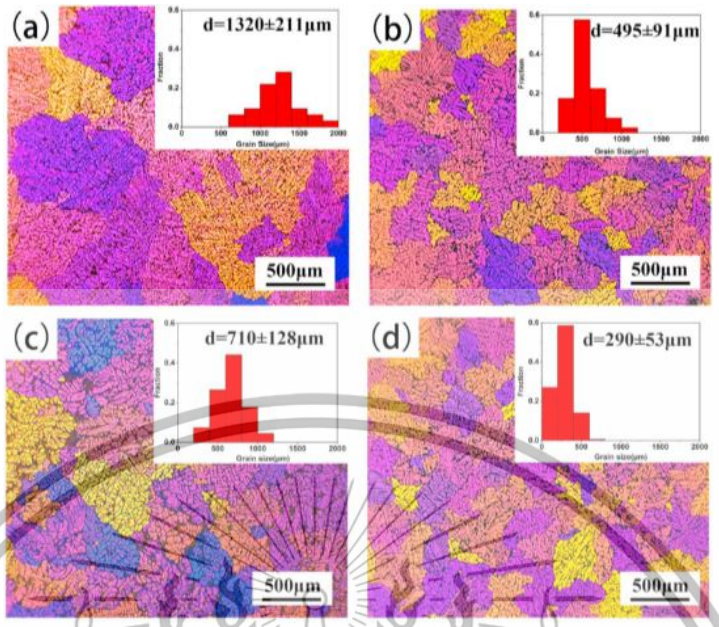

Figure 6 Representative optical micrographs and average grain size distributions of the as-cast (a) Al-5Ce, (b) Al-5Ce-0.2Zr, (c) Al-5Ce-0.2Sc, and (d) Al-5Ce-0.2Zr-0.2Sc alloys.

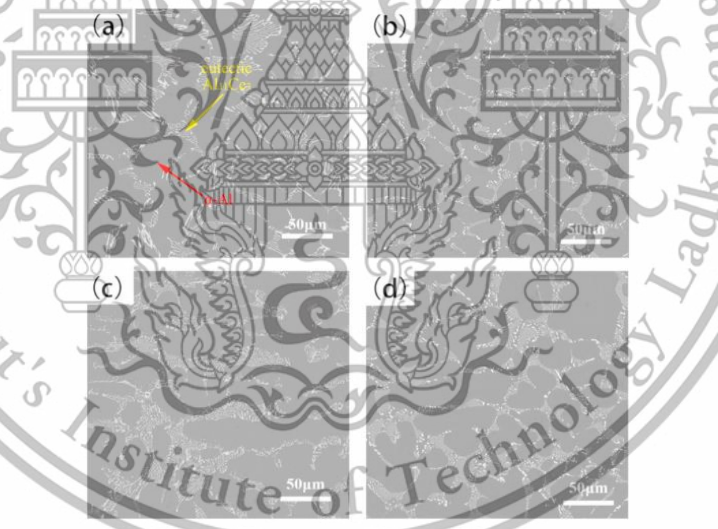

Figure 7 SEM images of the as-cast (a) Al-5Ce, (b) Al-5Ce-0.2Zr, (c) Al-5Ce-0.2Sc, and (d) Al-5Ce-0.2Zr-0.2Sc alloys.

The micrographs and average grain size distributions of as-cast Al-5Ce, Al-5Ce-0.2Zr, Al-5Ce-0.2Sc, and Al-5Ce-0.2Zr-0.2Sc alloys are presented in **Figure 6**. Dendritic substructures within grains are observed for all these alloys. The Al-5Ce alloy displays coarse equiaxed grains, as shown in **Figure 6 (a)** with an average size of about 1320 μm. Average grain sizes of 0.2Zr and 0.2Sc additions are 495 μm and 710 μm, respectively. The combined addition owns an average grain size of 290 μm, as shown in **Figure 6 (d)**. Zr and Sc additions remarkably refine the grain, and the 0.2Zr causes more obvious grain

refinement than 0.2Sc. Compared to the addition of 0.2Zr or 0.2 Sc, combined addition leads to a better refinement effect. Distributions of the eutectic $Al_{11}Ce_3$ phase in as-cast Al-5Ce and with 0.2Zr, 0.2Sc, and 0.2Zr + 0.2Sc additions are presented in **Figure 7**. Only the eutectic $Al_{11}Ce_3$ phase exists instead of the primary $Al_{11}Ce_3$ phase in these Al-Ce alloys, which is consistent with the Al-Ce phase diagram. The $Al_{11}Ce_3$ phase in Al-5Ce alloy distributes between coarse dendritic α-Al grains and dendrite arms, as shown in **Figure 7 (a)**. Compared to Al-5Ce base alloy, the eutectic $Al_{11}Ce_3$ phase segregation has noticeably reduced by adding 0.2Zr in **Figure 7 (b)**. As shown in **Figure 7 (c)**, adding Sc does not reduce segregation of the eutectic $Al_{11}Ce_3$ phase. It is seen in **Figure 7 (d)** that the microstructure homogenization effect of combined addition is between that of separate addition of 0.2Sc and 0.2Zr. Therefore, adding Zr is more effective than Sc in reducing the segregation of the eutectic $Al_{11}Ce_3$ phase. Therefore, the addition of 0.2Zr and 0.2Sc decreases the grain size, and combined addition exhibits the minimal grain size [16].

The introduction of the paper discusses the issue of most commercial aluminum alloys losing their strength above temperatures of 250 °C due to the coarsening and transformation of metastable precipitates. The paper specifically investigates the microstructural evolutions and associated hardening effects of cast and laser-surface-remelted Al-8Ce-0.2Sc-0.1Zr (wt.%) hypo-eutectic alloy, which contains Ce as a low-cost by product of rare-earth extraction and provides excellent castability when added to aluminum [16]. The addition of Scandium and Zirconium to this alloy forms Al_3(Sc, Zr) nanoprecipitates, which contribute to the hardening of the alloy. The paper finds that laser surface remelting suppresses the formation of undesirable primary $Al_{11}Ce_3$ and Al_3(Sc, Zr) precipitates on solidification and significantly refines the interlamellar spacing of the eutectic $Al_{11}Ce_3$ phase, thus enhancing the Orowan strengthening effect as compared to the cast alloy [16].

2.4 Ultrasonic Melt Treatment (UST)

Ultrasonic melt treatment (UST) is a process used in metallurgy to refine the microstructure of molten metals and alloys. It involves the application of high-frequency ultrasonic vibrations to the liquid metal, typically through an ultrasonic transducer or horn immersed in the melt. The vibrations create cavitation, the formation, growth, and collapse of tiny bubbles or voids in the liquid. During bubble collapse, localized high temperatures and pressures are generated, creating intense microstreaming and turbulence in the melt. These effects promote the removal of impurities, gas bubbles, and non-metallic inclusions, leading to a more homogeneous and refined microstructure in the solidified metal [17, 18].

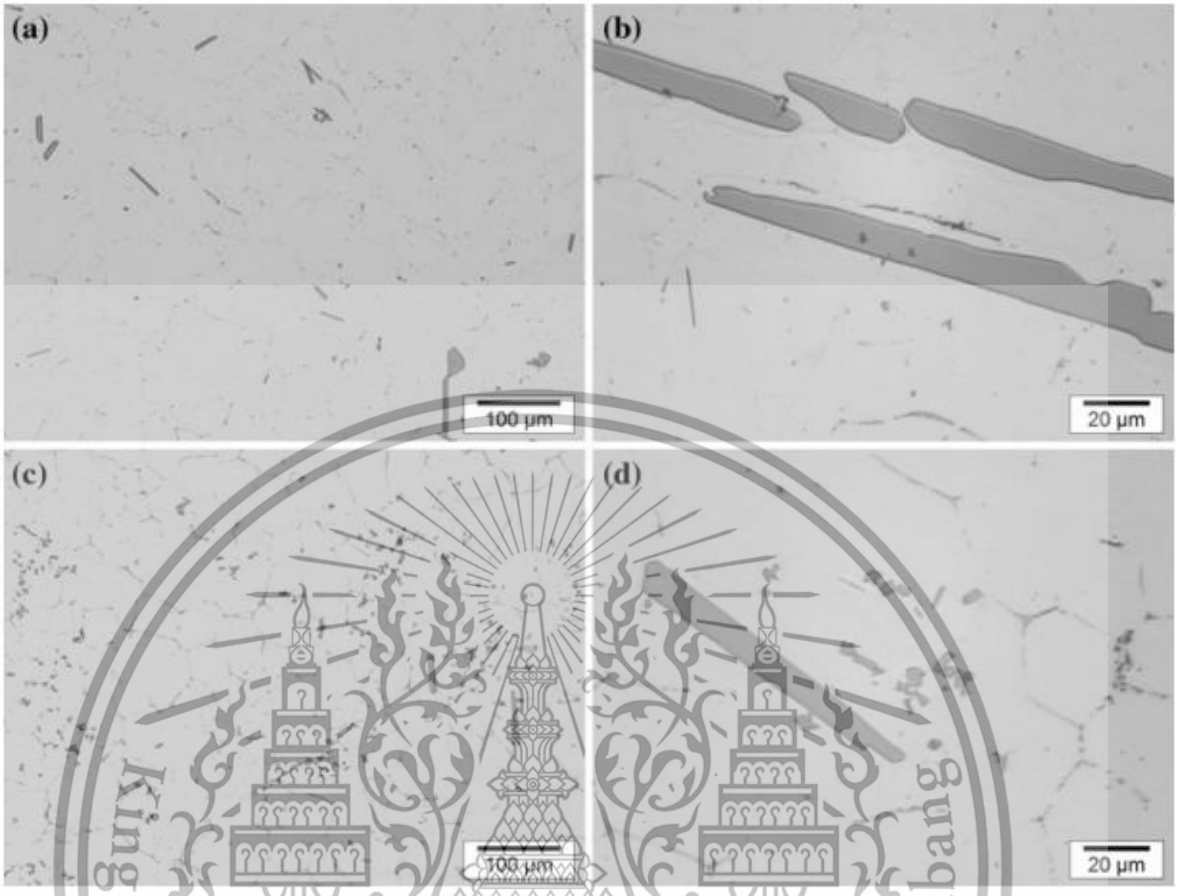

Figure 8 Morphology of primary intermetallic in the Al–0.4 wt.% Ti alloy (a, b) without ultrasonic melt treatment (c, d) with ultrasonic melt treatment.

It has been assumed and demonstrated that ultrasonic treatment causes primary intermetallic to fragment, increasing their number. Therefore, the Al-0.4 wt.% Ti alloy was subjected to UST in the solidification range of Al_3Ti to study the impact of UST on the formation of Al_3Ti and related grain refinement in a hyper peritectic Al-Ti alloy. The microstructures of the Al-0.4 wt.% Ti alloy without UST are shown in **Figure 8 (a)** and **Figure 8 (b)**. Al_3Ti particles ranged in size from 20 µm to 80 µm. As seen in **Figure 8 (c)**, two different types of Al_3Ti particles were discovered when UST was used. Most of the particles became dramatically more petite in size, ranging from 3 to 8 µm in **Figure 8 (d)**. The larger particles with a size range from 50 to 80 µm were fewer and are thought to form during solidification after UST [19].

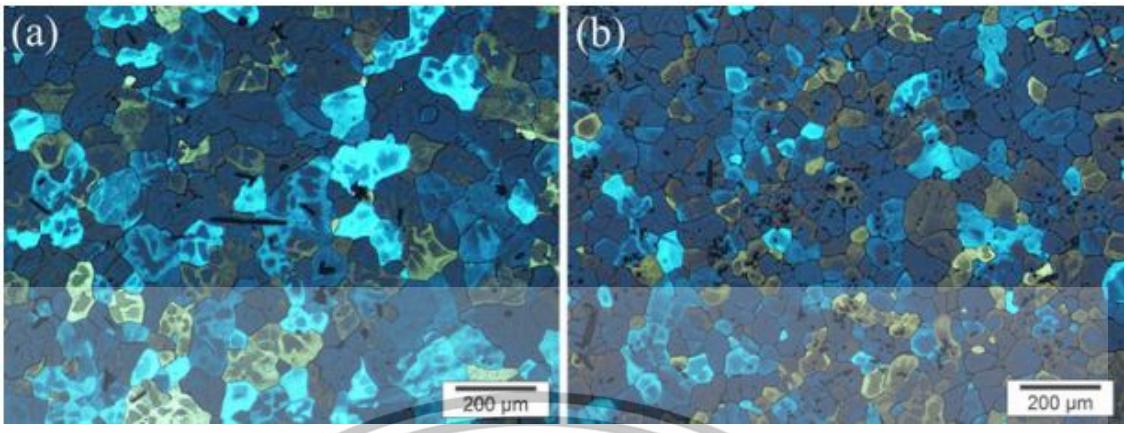

Figure 9 Effect of UST on the grain structure of the Al–0.4 wt.% Ti alloy (a) without UST (b) with UST.

The refinement of primary intermetallic resulted in the refining of Al grains, as shown in **Figure 9**. The grain size reduced from 90 µm to 65 µm when UST was applied to the Al–0.4 wt.% Ti alloy [19].

Figure 10 Morphology of primary intermetallic in the Al–0.4 wt.% Zr–0.12 wt.% Ti (a) without ultrasonic melt treatment (b) with ultrasonic melt treatment.

Figure 10 gives the overview of primary intermetallic in the Al–0.4 wt.% Zr–0.12 wt.% Ti alloy cast with and without UST. The results are similar to the Al–0.4 wt.% Ti alloy. The particle size was reduced from 50 µm to 100 µm without UST to 5–10 µm when UST was applied. However, contrary to the experiments with the Al–Ti alloys (Fig. 0000) and previous experiments, the grain size after casting in the graphite crucible increased from 115 µm without UST to 185 µm when UST was applied [19].

The benefits of ultrasonic melt treatment include grain refinement, homogenization of alloying elements, degassing to remove dissolved gases and removal of non-metallic inclusions. These improvements enhance the metal or alloy's mechanical and physical properties [17, 18].

2.5 Aging

In aluminum, the aging process is utilized to control the precipitation of particles in the solid state, thereby influencing the strength properties of the material. The effectiveness of aging depends on factors such as the size and dispersion of the particles. If the particle size is inadequate, it fails to contribute to improved durability during aging. Conversely, if the particles are too large, they become easily deformable, leading to decreased strength (Over-aging). In such cases, before the aging process, it may be necessary to subject the aluminum to a solution annealing treatment, which involves heating the metal to a temperature that allows improperly sized or dispersed particles to melt back into a homogeneous state. This solution annealing process helps ensure the desired particle size and distribution for effective strengthening [20].

Another aspect of hardening aluminum involves controlling the precipitation of particles during sintering, which is influenced by the desired particle size and sedimentation, often determined by the aluminum grade. Some aluminum grades, like 2024, exhibit natural aging, where precipitation can occur at room temperature. It is recommended to cold-shape aluminum of this grade within an hour of cooling or four days if it has not been forged to minimize the energy required for particle formation [21].

Furthermore, when the metal is heated, the precipitated particles can dissolve into the matrix. This phenomenon can be utilized for inducing controlled precipitation by subjecting the aluminum to artificial aging, typically at temperatures ranging from 100 to 200 °C. Although artificial aging offers advantages in manufacturing costs, it is essential to consider the temperature limitations to prevent excessive softening of the aluminum, which can result in reduced hardness [21].

According to EN 515, the aging state of aluminum is denoted by the letter T followed by a number, such as 2011-T8, 6061-T4, or 7075-T6. Sometimes, an additional digit provides more specific information about the hardening status and purpose. For example, T73 indicates an over-aged condition to prevent stress corrosion, while T76 signifies over-curing to prevent exfoliation corrosion, considering the material's strength properties. When selecting aluminum for use, it is essential to consider factors, for example, temperature and corrosion resistance, as heat treatment and aging not only affect strength but also indirectly influence other properties of aluminum [5].

Artificial aging is a process that transforms the supersaturated solid solution in aluminum alloys into precipitated particles, significantly enhancing the material's strength characteristics. Precipitation hardening is crucial in imparting the required mechanical properties for aerospace structures. Aging can occur naturally at room temperature or elevated temperatures through artificial aging. In most age-harden able alloys, natural aging is a gradual process, and its effects may not become noticeable for several months or even years [5].

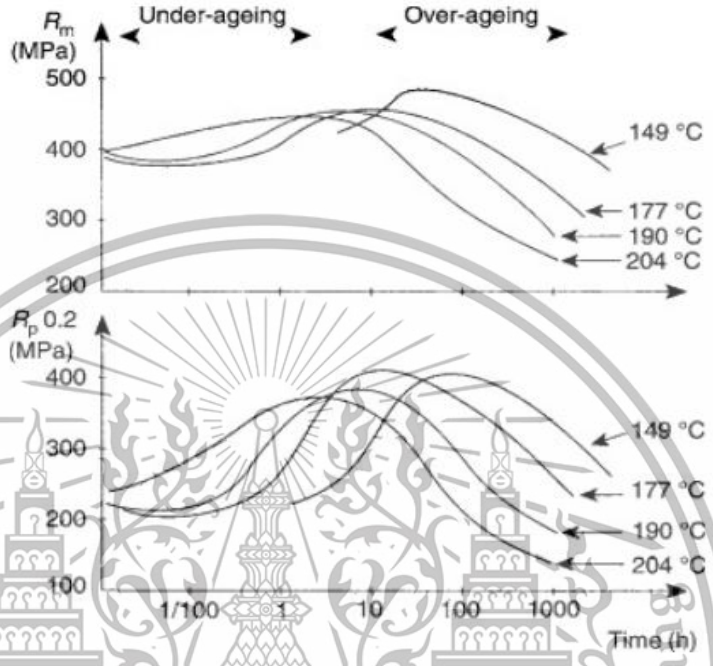

Figure 11 Aging treatment Al alloy.

Artificial aging is typically simulated using air furnaces. It is crucial to adhere to recommended time and temperature parameters to achieve the desired material characteristics, similar to the requirements for solution heat treatment. Each alloy has its specific set of artificial aging parameters, including temperature, duration, and the interval between quenching and aging [5].

The change in tensile strength over time during isothermal aging follows a bell-shaped curve, as depicted in **Figure 11**, with a peak value at a specific duration. Generally, alloys in artificially aged tempers may exhibit lower corrosion resistance than older tempers [5].

2.5.1 Role of alloying element in aging process

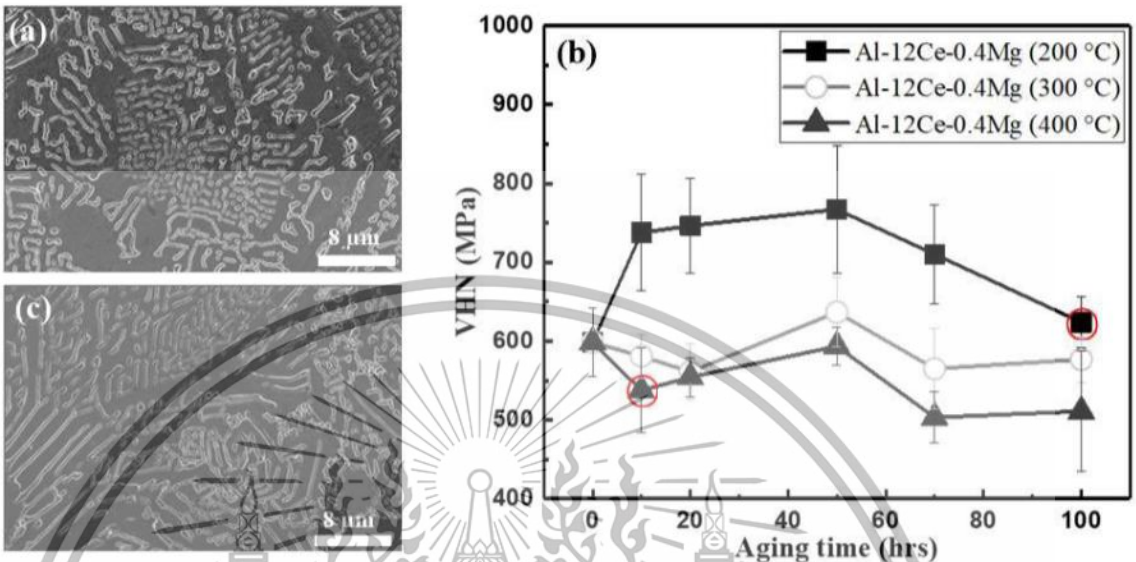

Figure 12 (a) The FESEM micrograph displays the transformation of lathes of intermetallic into spheroid particles through surface diffusion at 400 °C for 10 hours of aging time (b) Heat treatment study for Al-12Ce-0.4Mg alloy for different time intervals (0, 10, 20, 50, 70 and 100 hours) (c) long lathe-like intermetallic at 200 °C for 100 hours.

The paper discusses the mechanical properties and thermal stability of Al-12Ce-0.4Mg alloys. It has been reported that heat treatment at 400 °C for 10 hours transforms interconnected $Al_{11}Ce_3$ into discrete particles, resulting in a 10% decrease in hardness compared to the cast condition. The decline in hardness at 400 °C after 10 hours of heat treatment was attributed to the loss of solid solution strengthening and the release of strain energy. Heat treatment at 200 °C for 100 hours increases hardness by 23%, as shown in **Figure 12**, due to solid solution strengthening and load transfer capability. The addition of Mg alters the microstructure of the Al-Ce binary alloy, sacrificing some mechanical properties such as elongation percentage [14].

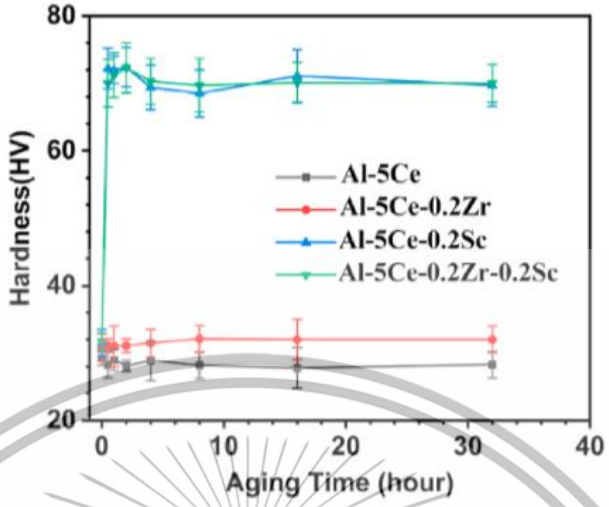

Figure 13 The graph illustrates the changes in hardness during isothermal aging at 350 °C for four different alloys: Al-5Ce, Al-5Ce-0.2Zr, Al-5Ce-0.2Sc, and Al-5Ce-0.2Zr-0.2Sc.

The research investigates the effect of micro-additions of Zr and Sc on the microstructure and mechanical properties of as-cast Al-5Ce alloy. Four alloys, Al-5Ce, Al-5Ce-0.2Zr, Al-5Ce-0.2Sc, and Al-5Ce-0.2Sc-0.2Zr, were produced by permanent mold casting using pure commercially available Al and master alloys. From **Figure 13**, it has been observed that the microhardness of four alloys was monitored during isothermal aging at 350 °C. Al-5Ce and Al-5Ce-0.2Zr alloys showed negligible age-hardening responses. Al-5Ce-0.2Sc and Al-5Ce-0.2Zr-0.2Sc alloys showed a remarkable increase in hardness due to the formation of Nano-sized Al_3Sc and $Al_3(Sc, Zr)$ particles [16].

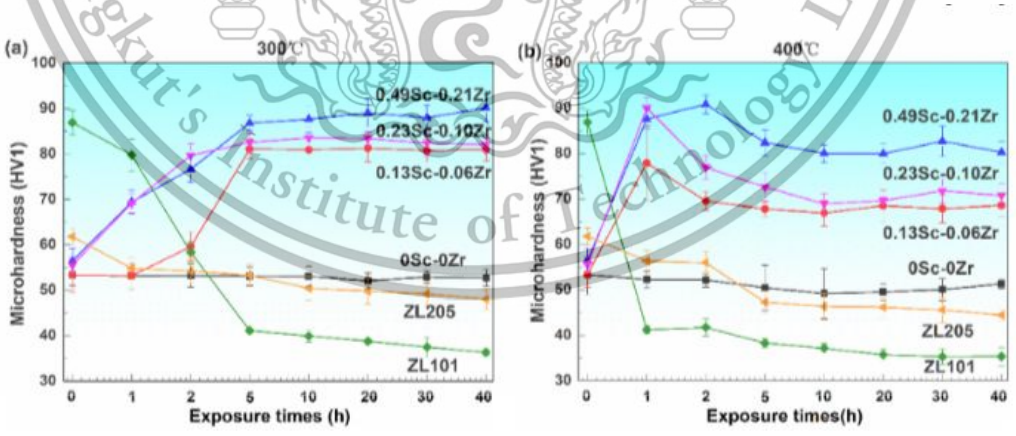

Figure 14 The microhardness measurements of Al-15Ce alloys with various Sc/Zr additions are shown after subjecting them to thermal exposure at elevated temperatures: (a) 300 °C and (b) 400 °C. The commercial ZL205 and ZL101 alloys are included as reference samples to assess the thermal stability at 300 °C and 400 °C, respectively.

The paper investigates the effect of Sc/Zr addition on the microstructure, mechanical properties, and thermal stability of a hyper eutectic cast Al-Ce alloy. The thermal stability of four alloys, including ZL101, ZL205, 0Sc-0Zr, and Sc/Zr-modified alloys, was evaluated through thermal exposure experiments, and the microhardness as a function of exposure time was measured. From **Figure 14**, for the reference alloys (ZL101 and ZL205), the microhardness decreased significantly with increasing holding time at elevated temperatures. After exposure at 300 °C and 400 °C for 40 hours, the microhardness declined by approximately 60% and 22-28%, respectively. In contrast, the 0Sc-0Zr alloy showed insignificant changes in microhardness with prolonged exposure time at 300 °C and 400 °C for 40 hours, with a value of approximately 53 HV1. The microhardness of three alloys with the addition of Sc/Zr, at 300 °C, increased with increasing exposure time, reaching a maximum after 5 hours and remaining stable for up to 40 hours. The microhardness values for these alloys reached approximately 80 HV1, 83 HV1, and 90 HV1, respectively. At 400 °C, the microhardness of the Sc/Zr alloys rapidly increased to a peak within 1 hour and then gradually decreased after 5 hours of exposure. However, the microhardness remained higher than the initial microhardness, with values of approximately 68 HV1, 70 HV1, and 80 HV1 after 40 hours of exposure. The presence of $Al_{11}Ce_3$ phases in this alloy enhanced its mechanical properties at elevated temperatures. This retention of considerable microhardness was attributed to the stability of $Al_{11}Ce_3$ phases and the precipitation hardening of Sc/Zr-rich phases in these alloys [22].

In summary, the Sc/Zr-modified alloys exhibited enhanced thermal stability, with microhardness either remaining unchanged or increasing at elevated temperatures compared to the reference alloys. The presence of $Al_{11}Ce_3$ and Sc/Zr-rich phases played a crucial role in improving the mechanical properties of these alloys at high temperatures [22].

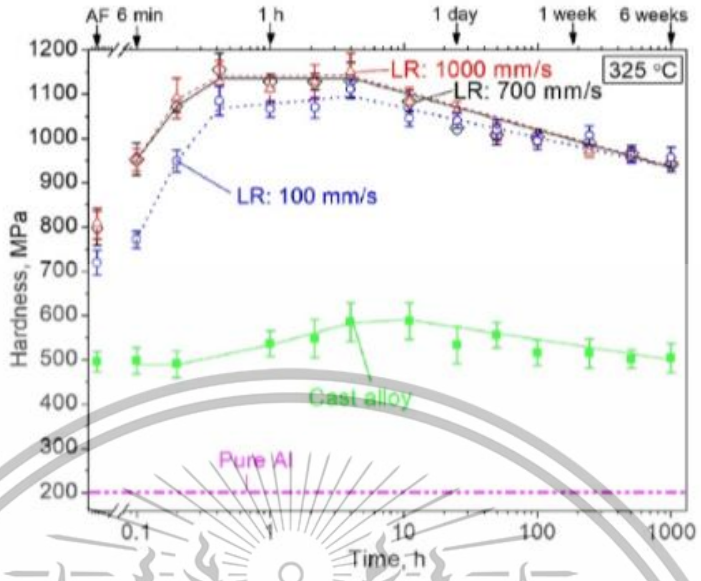

Figure 15 The evolution of hardness as a function of aging time is depicted for cast and laser-remelted (LR) Al-8Ce-0.2Sc-0.1Zr (wt.%) alloys at 325°C. The as-fabricated (AF) hardness values for both the cast and laser-remelted states are also presented.

The paper investigates the microstructural evolutions and associated hardening effects for both cast and laser-surface-remelted Al-8Ce-0.2Sc-0.1Zr (wt.%) hypo-eutectic alloy with a focus on precipitation and coarsening behavior of their $Al_{11}Ce_3$ precipitates. From **Figure 15**, the hardness of Al-8Ce-0.2Sc-0.1Zr alloys increases with an aging time up to 4 hours, then slowly decreases over time. The hardness of the Al11Ce3 precipitates is controlled by the size, number density, and volume fraction of Al3(Sc, Zr) secondary precipitates forming on aging. The as cast Al–8Ce-0.2Sc-0.1Zr (wt.%) reached its peak hardness after four hours of aging at 325 °C, in agreement with other L12-strengthened cast Al(-Mg)-Sc alloys aged at 300 or 350 °C [17].

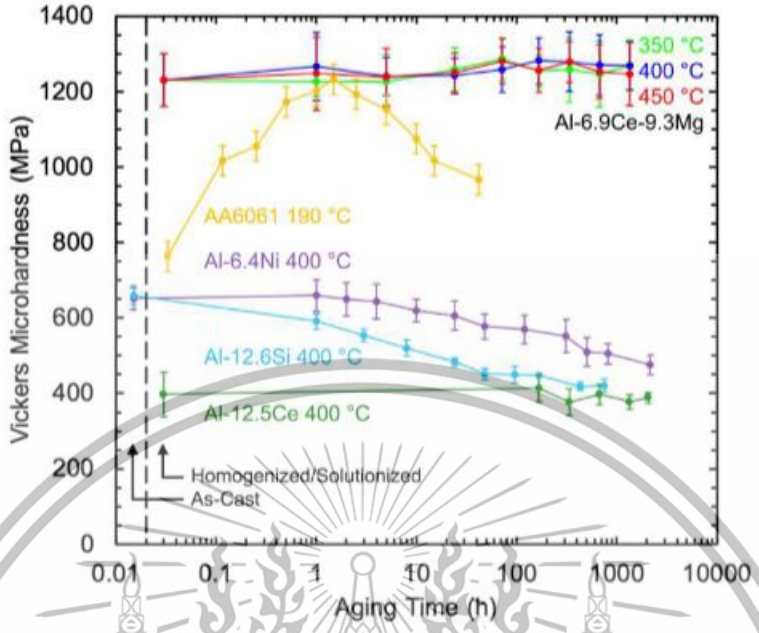

Figure 16 The Vickers microhardness of the eutectic Al (Mg)-$Al_{11}Ce_3$ regions in the Al-6.9Ce-9.3Mg (wt.%) alloy as a function of isothermal aging time at 350, 400, and 450°C for a duration of up to 8 weeks (1344 hours).

The current study examines the coarsening resistance and mechanical characteristics of a cast Al-6.9Ce-9.3Mg (wt.%) hypoeutectic alloy composed of an -Al matrix with Mg in solid solution and embedded eutectic colonies containing a fine distribution of highly branched $Al_{11}Ce_3$ phase, with a volume fraction of about 15%. A combination of factors, solid-solution strengthening from the high (11.2 wt.%) Mg content in the matrix, precipitation strengthening from the $Al_{11}Ce_3$ phase, and load-transfer strengthening from the $Al_{11}Ce_3$ phase, may explain why the ternary alloy's Al (Mg)-$Al_{11}Ce_3$ eutectic microstructure has a relatively high Vickers microhardness of 1230 70 MPa as shown in **Figure 16**. The ternary alloy has a hardness of 400–60 MPa, significantly higher than the binary near-eutectic Al–12.5Ce alloy. Al (Mg)-$Al_{11}Ce_3$ eutectic areas' microhardness and morphology show exceptional coarsening resistance after 8 weeks (1344 h), even at temperatures as high as 450 °C [12].

The ternary Al-6.9Ce-9.3Mg alloy has better creep resistance than an Al-5.0Mg solid-solution reinforced alloy but is less resistant than an Al-12.5Ce near-eutectic alloy. In agreement with the hypoeutectic ternary alloy's intermediate creep performance, a creep activation energy of 246 23 kJ/mol, which is significantly higher than the value for dislocation creep but similar to that of the Al-12.5Ce near-eutectic alloy, suggests that the eutectic microstructure significantly influences creep behavior through both precipitate and composite strengthening [12].

2.6 Brinell hardness machine

In the Brinell hardness test, a sintered carbide test ball is pressed against the material, and the impression is then assessed. Initially, test balls made of steel or hardened metal were employed. These are, however, no longer accepted as of 2006. Since then, only hard metal balls have been utilized for hardness testing. The test ball's diameter ranges from 10 mm to 5 mm to 2.5 mm to 2 mm or even 1 mm. The type of ball to use depends on the thickness of the material to be examined. Depending on the type of cloth, the typical pressing time is 10 to 15 seconds. The exposure period can potentially be extended up to 30 seconds for materials that are extremely soft [23].

Figure 17 Brinell hardness test machine.

For the Brinell hardness test, care must be taken to ensure that the material being tested has a clean, flat, impurity-free surface. The test ball's vertical penetration and shock-free penetration must also be taken into consideration. After the compressive load, the impression's vertical and horizontal diameters are measured. The average value is calculated using these two values, and the diameter is then utilized to calculate the Brinell hardness in the appropriate way. In HBW, which stands for Hardness, the Brinell hardness is expressed [24].

The following is the formula for determining Brinell hardness:

$$HB = \frac{2P}{\pi D\left(D - \sqrt{D^2 - d^2}\right)}$$

where

- HB = Brinell Hardness Number (kgf/mm^2)
- P = applied load in kilogram-force (kgf)
- D = diameter of indenter (mm)
- d = diameter of indentation (mm)

Over the years, two different technology solutions to Brinell's measurement error issues have been created. Automatic optical Brinell scopes, like the B.O.S.S. system, read the indentations consistently using computers and image analysis. This standardization helps eliminate operator subjectivity so operators are less-prone to automatically view in-tolerance results when the sample's result may be out-of-tolerance [24].

2.7 Tensile test

A significant factor in material science and engineering is the controlled tension test, which involves putting a sample under stress until it fails. A tensile test can be used to determine parameters such as maximum elongation, area reduction, ultimate tensile strength, and breaking strength. These findings can be used to compute Young's modulus, Poisson's ratio, yield strength, and strain-hardening properties. Uniaxial tensile testing is the most common technique for assessing the mechanical characteristics of isotropic materials. Some materials are subjected to biaxial tensile testing. Different testing equipment dramatically alters how the load is given to the materials [25].

There are three types of tensile strength:

1. A material's yield strength is its capacity to withstand stress without permanently deforming it.
2. The maximum stress that a material can withstand is known as ultimate strength.
3. The stress that is coordinated on the stress-strain curve at the point of rupture is known as the breaking strength.

Tensile strength, a constrained state of tensile tension, can fail in one of two ways:

1. Failure of a duct - The initial step of failure is yield, the second stage involves some hardening, and the last stage is breaking following potential "neck" formation.
2. brittle failure - The breaking into two or more pieces while under minimal stress.

When metals are subjected to a tensile strength test, it may be determined how much an alloy will elongate before achieving its maximum tensile strength and how much load a specific metal piece can support before losing structural integrity. For this reason, it's crucial to understand a material's tensile strength for construction and personal safety. Tensile strength, corrosion resistance, and elastic modulus are crucial characteristics of materials used in mechanical devices and structures. It includes wood, ceramics, polymers, composite materials, metals, and other building-related materials [26].

The tensile test is used to provide data for design calculations or to show that a material conforms with the specifications of the relevant specification; as a result, it can be either a quantitative or a qualitative test. In order to do the test, you first grab the ends of a standard test piece that has been properly prepared and standardized in a tensile test machine. Next, you must apply a continuously rising uni-axial force until failure is reached. To ensure that results are repeatable and comparable, test items are standardized [26].

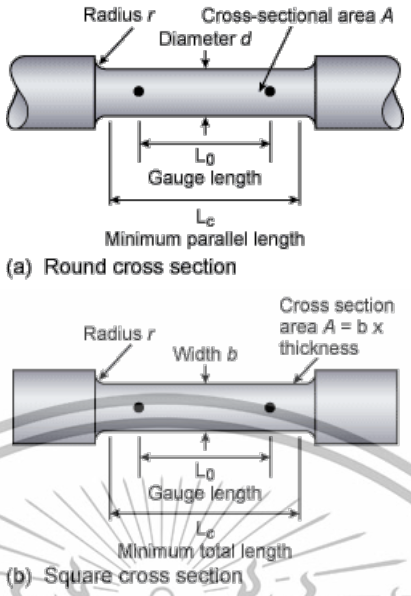

Figure 18 Standard shape tensile specimens.

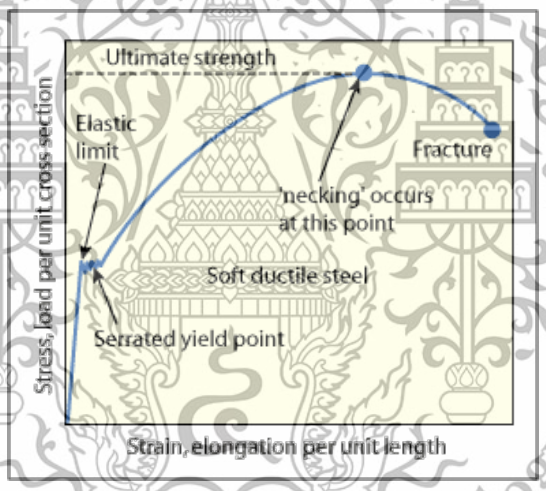

Figure 19 Stress/strain curve.

When using specimens that are said to be proportional, the gauge length, L0, is related to the original cross-sectional area, A0, according to the equation $L0 = k\sqrt{A0}$. The value of the constant k differs depending on the specifications used: 5.65 in EN specifications and 5 in the ASME codes. These values result in gauge lengths approximately 5 times the specimen diameter and 4 times the specimen diameter, respectively. Using the load (stress) and test piece extension (strain) data obtained from the proportional specimens, an engineering stress/strain curve can be constructed as shown in **Figure 18** and **Figure 19.**

1. The load at failure divided by the initial cross-sectional area yields the tensile strength, commonly known as the ultimate tensile strength (UTS). The maximum load is P_{max}, and the initial cross-sectional area is A_0. "R_m" is another term for this parameter in EN standards; [27].

2. The yield point (YP), also known as the stress at which deformation switches from elastic to plastic behavior, is defined as the point below which unloading the specimen causes it to return to its original length and above which permanent plastic deformation has taken place. The yield point is defined as $y = P_{yp} / A_0$, where P_{yp} is the load at the yield point. This parameter is also known as "R_e" in EN standards; [27].
3. The gauge length at fracture and the original gauge length can be used to calculate the percentage elongation, or El%, which indicates how much the test piece has stretched at failure. $El\% = (L_f - L_0 / L_o) \times 100$. This parameter is also known as "A" in EN standards. [27].
4. R of $A\% = (A_0 - A_f / A_0) \times 100$, where A_f is the cross-sectional area at the site of the fracture, is a measure of how much the specimen has necked or shrunk in diameter at the point of failure. This parameter is also known as "Z" in EN standards [27].

CHAPTER 3 EXPERIMENT PROCEDURE

3.1 Introduction

This chapter will include a characterization of the microstructure, a discussion of the tensile testing and hardness testing method used to determine the mechanical properties of the alloys investigated, as well as all the necessary details about the alloys used in the current research. It will also provide a description of the general melting and casting procedures used. **Table 4** provides a detailed description of the additions made in each case.

Table 4 Chemical composition

Alloys	Ce	Mg	Zr	Sc	Al
	wt.%	wt.%	wt.%	wt.%	wt.%
Al-15Ce (High cooling rate)	15	-	-	-	Bal.
Al-15Ce-0.75Mg (High cooling rate)	15	0.75	-	-	Bal.
Al-15Ce-0.75Mg-0.2Sc-0.2Zr (High cooling rate)	15	0.75	0.2	0.2	Bal.
Al-15Ce (Low cooling rate)	15	-	-	-	Bal.
Al-15Ce-0.75Mg (Low cooling rate)	15	0.75	-	-	Bal.
Al-15Ce-0.75Mg-0.2Sc-0.2Zr (Low cooling rate)	15	0.75	0.2	0.2	Bal.

3.2 Alloy preparation and melting procedures

3.2.1 Material used in the casting process

1. Aluminum 100% weight
2. Aluminum 20% weight of cerium
3. Magnesium 100% weight
4. Aluminum 2% weight of scandium
5. Aluminum 10% weight of zirconium

3.2.2 Equipment and machine used in experiment

1. Electric induction furnace
2. Silicon Carbide (SiC) crucible
3. Ultrasonic machine
4. Cutting machine
5. Sandpaper with a grit size of 180, 240, 360, 480, 600, 800, 1000, and 1200.
6. 3-micron polishing disc
7. Ops polishing disc
8. Alcohol
9. Barker acid ($HBF_4 + H_2O$)
10. Belt sander
11. Rotary disc sander
12. Optical microscope
13. Scanning electron microscope
14. Rigaku SmartLap SE X-ray diffractometer machine
15. NEXUS 3200 Brinell hardness testing machine
16. Shimadzu AXG-V2 Tensile testing machine

3.3 Melting and casting procedures

1. The preheated furnace at a temperature of 300 °C was used to help to manage thermal conditions, improve metal flow, and achieve a better surface finish.
2. The alloys were heated to 850 °C in an electric induction furnace using Silicon Carbide crucibles to melt them.
3. For the melt without ultrasonic treatment, the melt was poured into a Silicon Carbide crucible directly at a temperature of 720 °C.
4. From a temperature of 740 °C to 720 °C, the alloy composition was performed ultrasonic treatment by using ultrasonic machine with 19.5 kHz frequency. The melt was poured into a Silicon Carbide crucible after UST.

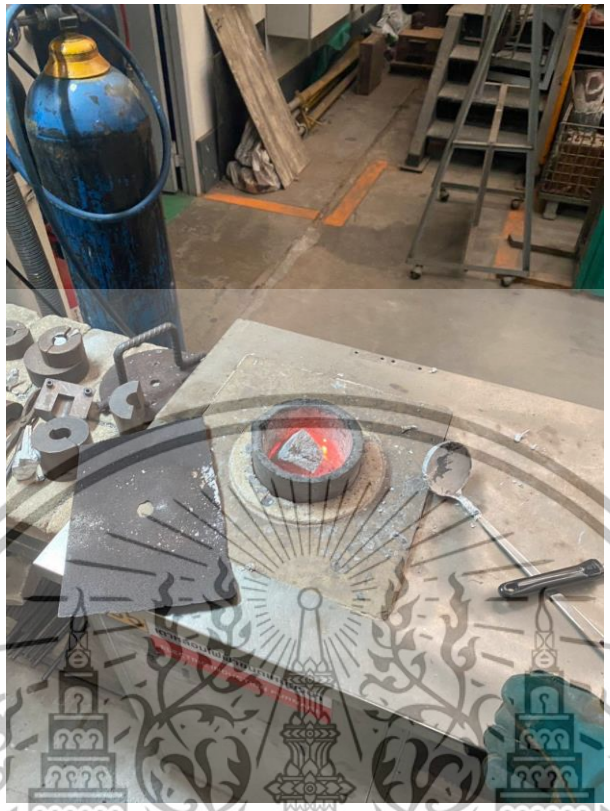

Figure 20 Melting aluminum.

Figure 21 Ultrasonic machine.

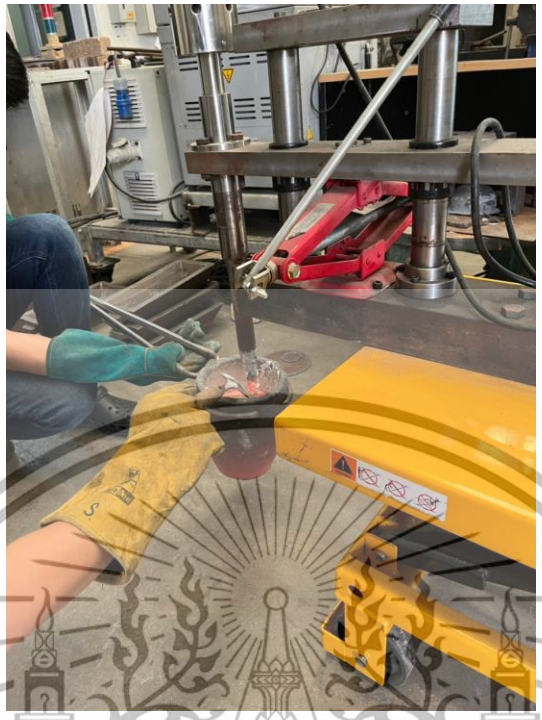

Figure 22 Ultrasonic process.

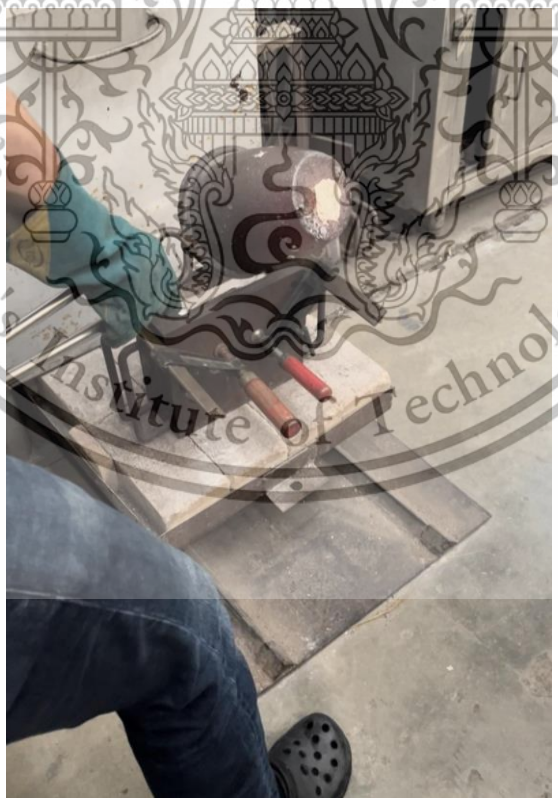

Figure 23 Pouring.

3.4 Heat treatment procedures

Al-15Ce, Al-15Ce-0.75Mg, and Al-15Ce-0.2Zr-0.2Sc will be aged for 30 hours. The specimens were aged at 150, 175, and 350 °C. The Brinell hardness machine will be used to measure the hardness every three hours.

3.5 Metallography

To observe and analyze the microstructure of each of the workpieces to study the effect of adding elements to the microstructure of aluminum cerium alloys.

1. The piece of work will be split up into smaller pieces and grinding with sandpaper with a grit size of 180, 240, 360, 480, 600, 800, 1000, and 1200.
2. The workpiece will then be polished using a 3-micron polishing disc.
3. The workpiece will then be polished using an OPS polishing disc.
4. The microstructure observes using 5x, 10x, and 20x magnifications.

3.6 Scanning Electron Microscope (SEM)

In an electron microscopic structural analysis, it is to inspect the microstructure of the workpiece. Energy-dispersive X-ray spectroscopy (EDS) mapping also use to obtain elemental composition information and spatial distribution of elements within alloys.

1. Bring the workpiece to polish with sandpaper with a grit size of 180, 240, 360, 480, 600, 800, 1000, and 1200 then polish with 3-micron polishing disc and Ops polishing disc, respectively.
2. Rinse with clean water and spray ethanol on the work piece, then blow it with hot air.
3. The workpiece is photographed to analyze the structure of the elements that appear in the microstructure.

3.7 X-ray diffractometer (XRD)

Take a test specimen with a thickness of 0.5 cm to study the crystal structure through the process of an X-ray diffractometer. The results obtained from XRD (SmartLab SE) are used to analyze the composition of the internal structure of the workpieces.

3.8 Image-J Program

To analyze the data of macrostructure, grain size, and microstructure photographs, the Image-J program was used to analyze the photographs.

1. Open the Image J program and select the image file to be analyzed.
2. Choose straight line command (Straight), then drag a straight line along the scale line (Scale) to set the scale from pixel units to a real unit of length.
3. Choose the Analyze > set scales command. A window will appear, then enter the length in the known distance field, and in the unit of the length field, adjust in micrometers. as shown, then press OK.
4. Select the Image > Adjust command, then adjust the Brightness / Contrast to reduce noise from the photo, then press Set.
5. Select straight line command (Straight) to measure, then press Ctrl + M to measure.
6. Repeat step 1 to 5 until the entire image file is analyzed. and taken for further analysis.

3.9 Hardness test

To measure and analyze the effect of adding elements to aluminum cerium alloy's hardness of each of the workpiece conditions.

1. The workpiece will be cut into small pieces and grinding using sandpaper with grits ranging from 180 to 800.
2. Brinell hardness tester will press the sample. Five different places on the workpiece by using a 2.5 mm ball head and a 62.5 kgF force load.
3. using a camera to gauge the indentation's diameter. The machine will measure the hardness value.

Figure 24 Brinell hardness machine.

3.10 Tensile test

Testing by using a tensile force to pull the material slowly makes the material hold longer and may give more and more tensile strength. until the test piece is broken then record the relationship between the tensile stress and the tensile strain and show the relationship in a graph called a stress-strain curve.

1. Preparation of the test specimens, the simple is then machined into a rectangle by electrical wire cutting. The rectangle specimens for following tensile testing were manufactured according to the ASTM B557 with gauge length 25 mm, thickness 6mm as shown in **Figure 25**.
2. Aging test specimens in 150 and 350 °C in each composition before tensile testing at room temperature.
3. Set the tensile machine (Shimadzu AXG-V2) to determine the Yield strength, Elongation, Ultimate tensile strength and Stress-Strain curve. The machine is set according to the requirements of the test including testing speed, gauge length.
4. The tensile test is conducted by slowly applying a tensile load to the specimen. The load is increased gradually, and the deformation of the specimen is measured continuously. The test is continued until the specimen fractures or until a predetermined strain or stress value is reached.
5. The data is analyzed to determine the mechanical properties of the material. The yield strength is determined from the stress-strain curve as the stress at which the material begins to deform plastically. The ultimate tensile strength is the maximum stress that the material can withstand before it fractures. The modulus of elasticity is the slope of the stress-strain curve in the elastic region.

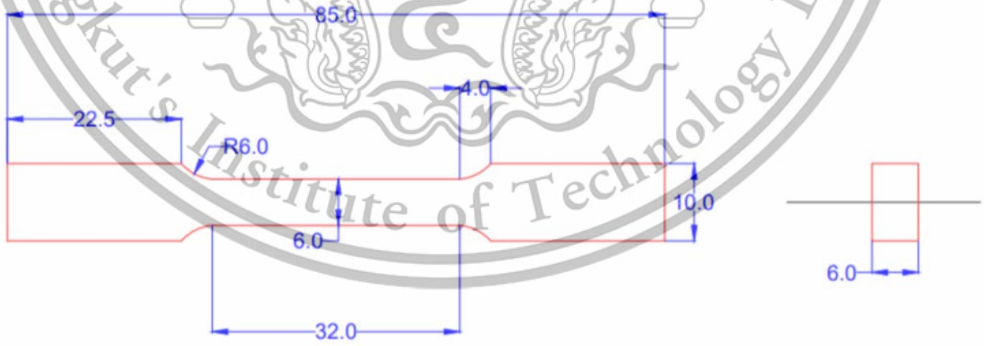

Figure 25 Tensile Model.

Chapter 4 RESULT AND DISCUSSION

In this chapter, the microstructure of Aluminum Cerium alloy with adding elements and different cooling rates is studied using optical and electron microscopy. In addition, energy-dispersive X-ray mapping was implemented to show the chemical composition distribution in the material. Also, X-ray diffraction identified the distinct phases in the material. Besides studying the microstructure of alloys, the mechanical properties and effect of heat treatment on the alloy characteristics were also studied.

4.1 Microstructure of Al-15Ce

Based on the study of the microstructure of the Aluminum Cerium alloy using a microscope, their microstructures mainly consist of the intermetallic compound, unevenly distributed on the aluminum substrate and eutectic phase, as shown in **Figure 26**.

The result of the macrostructure of the Al-15Ce alloy showed a large eutectic grain structure, which was reduced in size upon the addition of magnesium as shown in **Figure 27** and **Figure 28**, increasing the number of intermetallic particles. In addition, the addition of 0.2 wt.% Scandium and zirconium led to the formation of smaller, finer intermetallic particles and decreased eutectic phases, as observed in **Figure 26**.

The microstructural characterization of aluminum cerium alloy (Al-15Ce) and its modification with magnesium and scandium-zirconium alloys demonstrated a significant influence on the grain and intermetallic structures of the material, indicating the potential for optimizing the material properties.

Figure 26 shows that the Al- 15Ce alloy with ultrasonic treatment has a smaller size of intermetallic and grain than the Al-15Ce alloy without ultrasonic treatment. Ultrasonic treatment lead to grain refinement in metals and alloys. The high-frequency vibrations generated by ultrasonic waves can disrupt grain boundaries and promote the formation of smaller grains [28]. This refinement often improves mechanical properties such as increased hardness and strength. Ultrasonic treatment can increase the dislocation density in materials [28]. The high-frequency vibrations can introduce additional dislocations, enhancing the strain-hardening response and improving the material's strength and hardness [28].

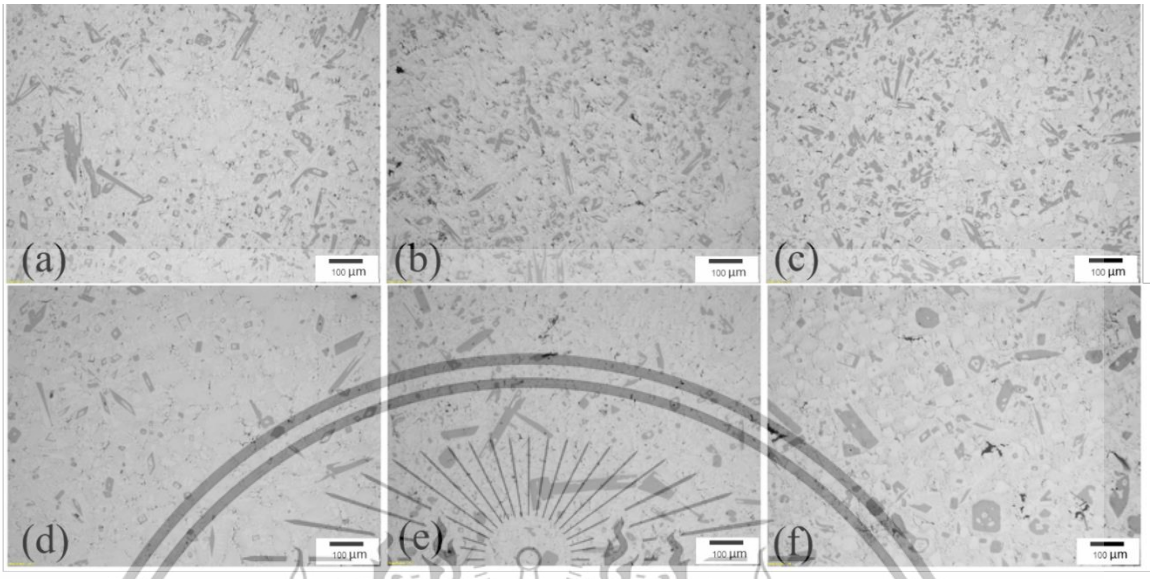

Figure 26 Optical micrograph of as-cast (a) Al-15Ce, (b) Al-15Ce-0.75Mg, (c) Al-15Ce-0.75Mg-0.2Sc-0.2Zr alloys with high cooling rate and (d) Al-15Ce, (e) Al-15Ce-0.75Mg and (f) Al-15Ce-0.75Mg-0.2Sc-0.2Zr alloys with low cooling.

4.2 Effect of cooling rate on microstructures

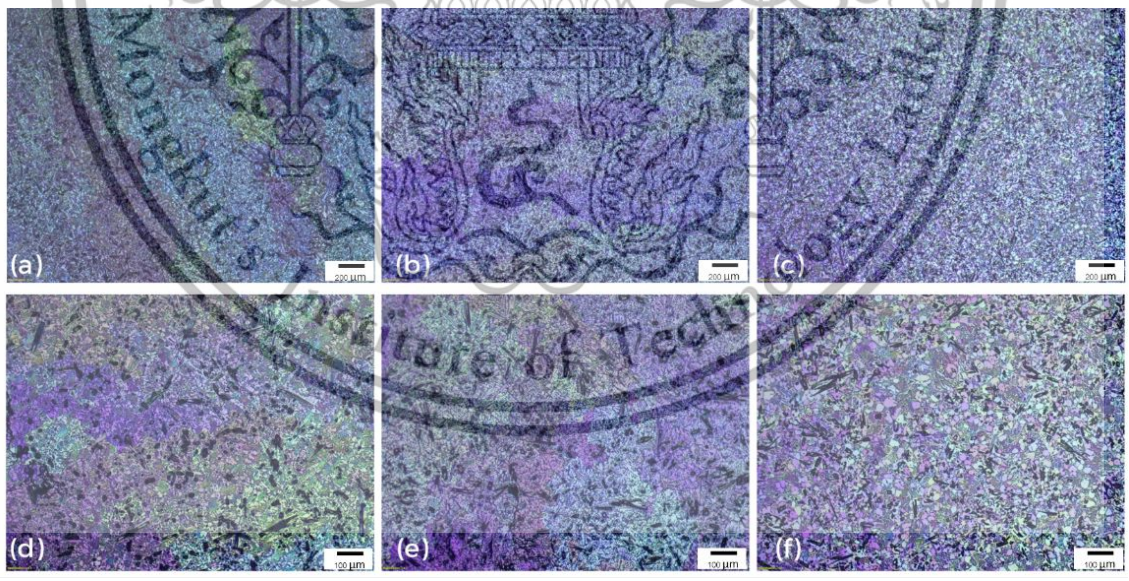

Figure 27 Grain structure of as-cast (a, d) Al-15Ce, (b, e) Al-15Ce-0.75Mg and (c, f) Al-15Ce-0.75Mg-0.2Sc-0.2Zr alloys with high cooling rate.

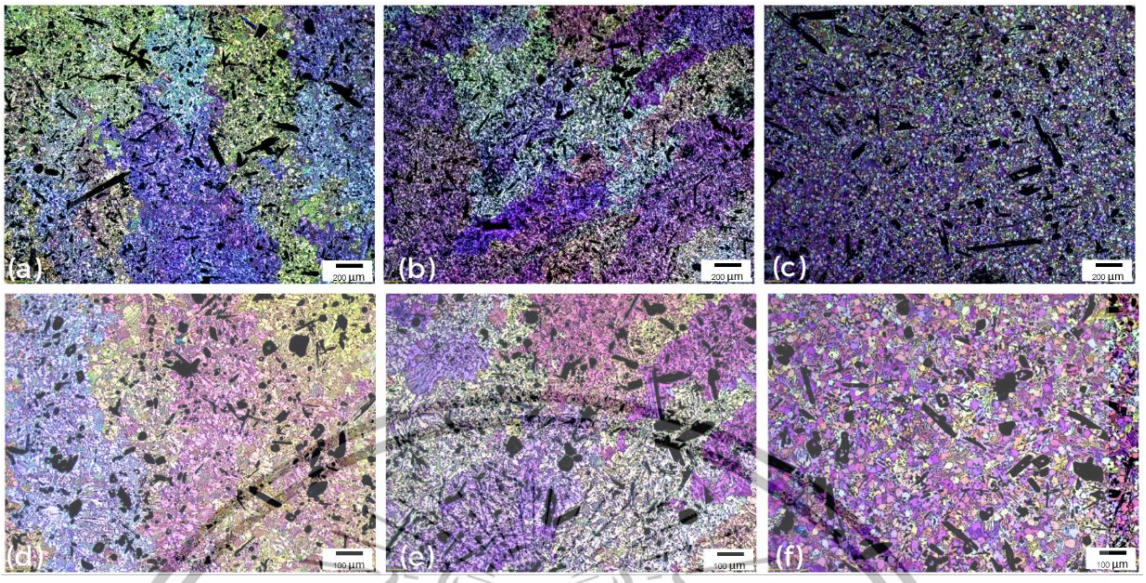

Figure 28 Grain structure of as-cast (a, d) Al-15Ce, (b, e) Al-15Ce-0.75Mg and (c, f) Al-15Ce-0.75Mg-0.2Sc-0.2Zr alloys with low cooling rate.

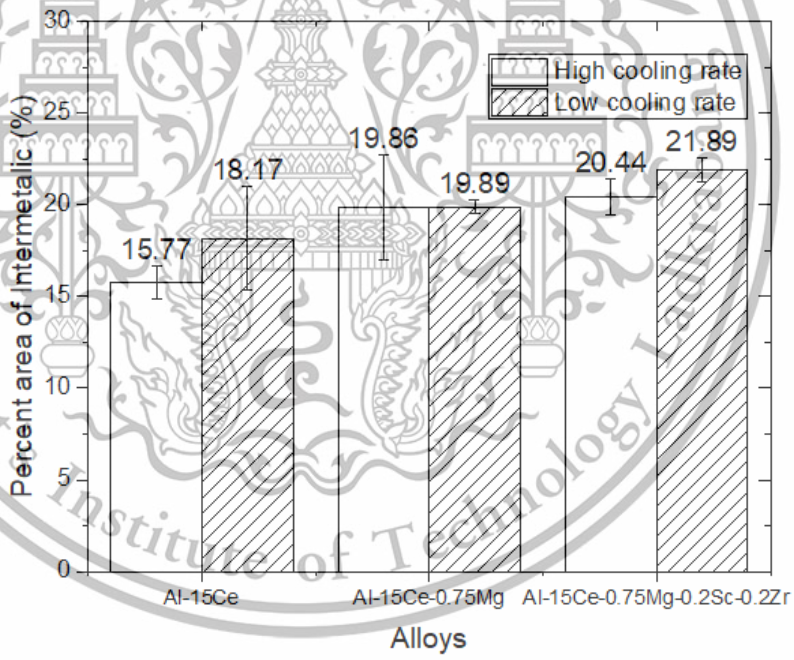

Figure 29 Percent area of intermetallic with different cooling rate.

High cooling rate

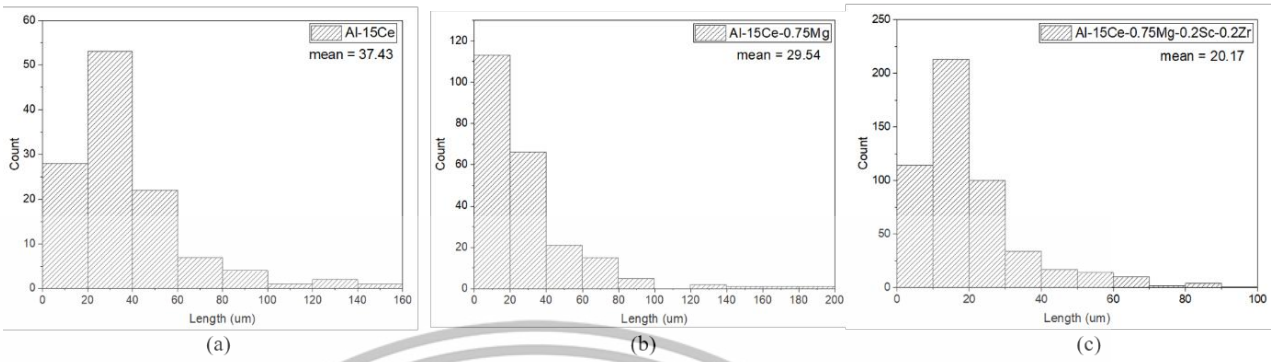

Figure 30 Intermetallic size distribution of as-cast (a) Al-15Ce, (b) Al-15Ce-0.75Mg and (c) Al-15Ce-0.75Mg-0.2Sc-0.2Zr alloys with high cooling rate.

Low cooling rate

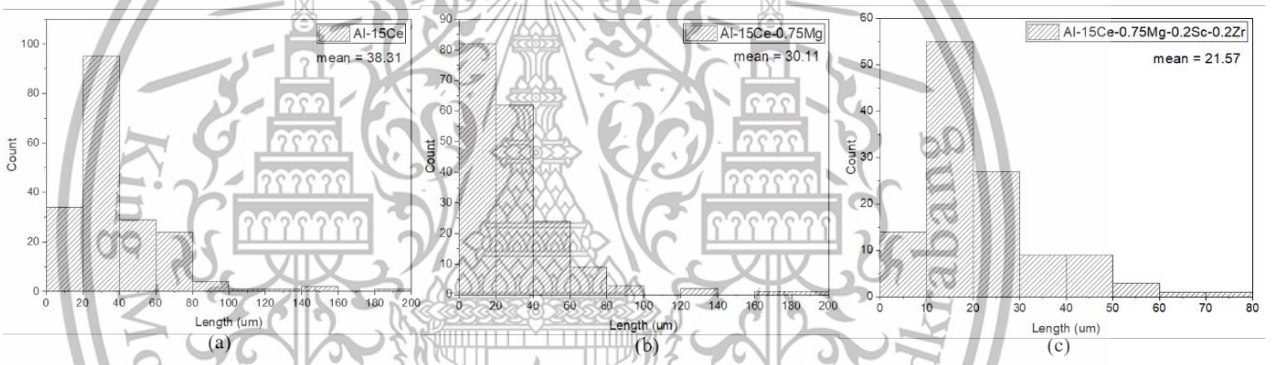

Figure 31 Intermetallic size distribution of as-cast (a) Al-15Ce, (b) Al-15Ce-0.75Mg and (c) Al-15Ce-0.75Mg-0.2Sc-0.2Zr alloys with low cooling rate.

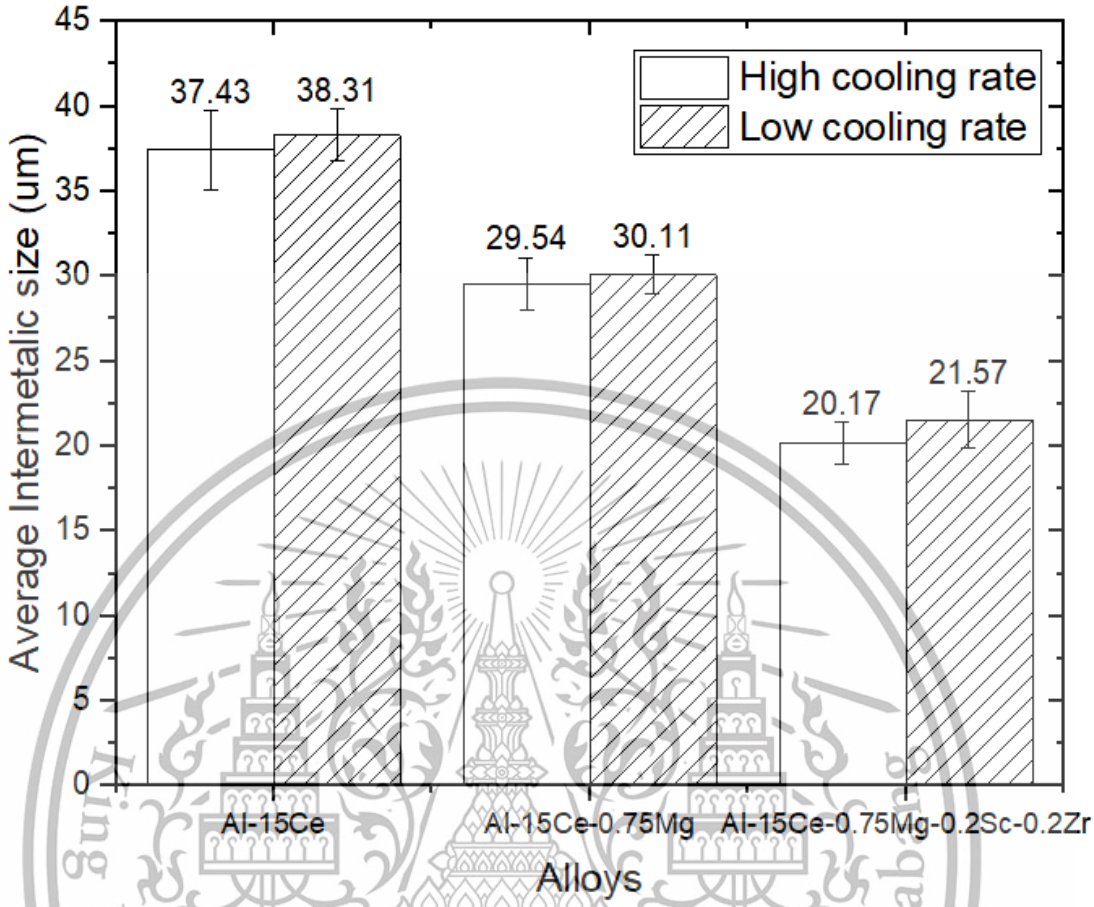

Figure 32 Average intermetallic size of Al-15Ce, Al-15Ce-0.75Mg and Al-15Ce-0.75Mg-0.2Sc-0.2Zr alloys with different cooling rate.

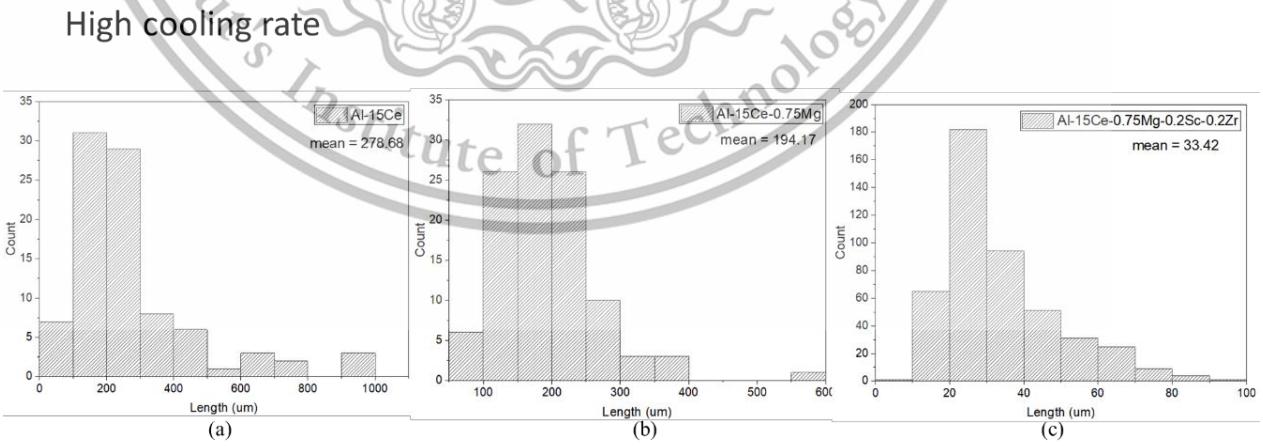

Figure 33 Grain size distribution of as-cast (a) Al-15Ce, (b) Al-15Ce-0.75Mg and (c) Al-15Ce-0.75Mg-0.2Sc-0.2Zr alloys with high cooling rate.

Low cooling rate

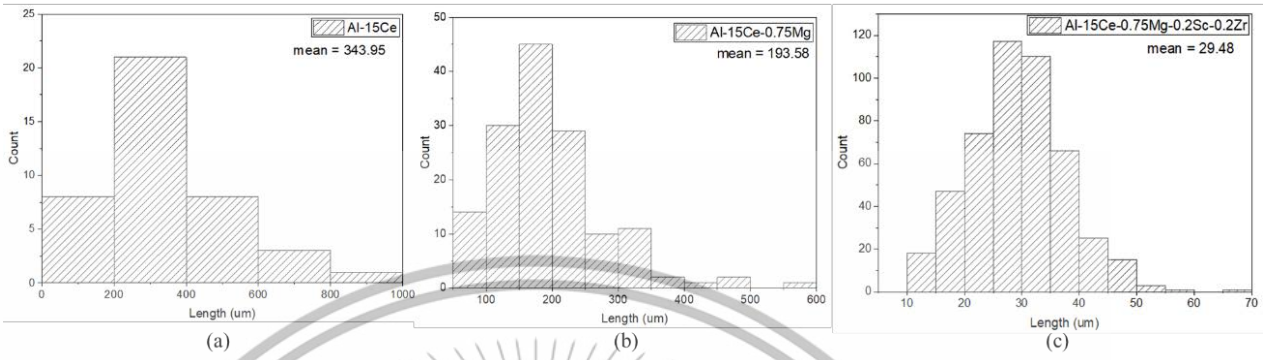

Figure 34 Grain size distribution of as-cast (a) Al-15Ce, (b) Al-15Ce-0.75Mg and (c) Al-15Ce-0.75Mg-0.2Sc-0.2Zr alloys with low cooling rate.

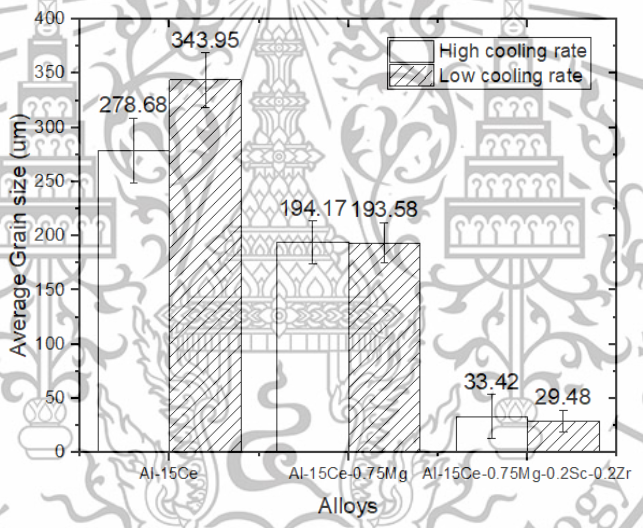

Figure 35 Average grain size of Al-15Ce, Al-15Ce-0.75Mg and Al-15Ce-0.75Mg-0.2Sc-0.2Zr with different cooling rate.

The result of measuring the proportion of distribution of metallic compounds on the surface of aluminum found that Aluminum alloy with a low cooling rate has more percent of intermetallic more than a high cooling rate, as shown in **Figure 29.**

The graph in **Figure 30**, **Figure 31**, and **Figure 32** displays the distribution and average intermetallic size of alloys with different cooling rates. The graph shows that the average intermetallic size of a low cooling rate is larger than a high cooling rate. The cooling rate during the solidification process affects the size and distribution of intermetallic particles in Al-15Ce alloys.

In Al-15Ce alloys, the intermetallic particles typically comprise cerium (Ce) and other alloying elements, such as aluminum (Al), which form complex intermetallic compounds.

These compounds can play a crucial role in the mechanical properties of the alloy, as they can act as both strengthening agents and potential sources of cracking and failure. When Al-15Ce alloys are cooled slowly, the intermetallic particles have more time to grow and coarsen. This can result in larger particles that can reduce the ductility and toughness of the alloy. Moreover, larger intermetallic particles can also act as potential sites for crack initiation and propagation, reducing resistance to cracking and failure [29].

In contrast, when Al-15Ce alloys are cooled rapidly, the intermetallic particles have less time to grow and coarsen. This can result in smaller particles that can enhance the ductility and toughness of the alloy. Smaller intermetallic particles also tend to be more homogeneously distributed in the matrix, which can lead to a more uniform strengthening effect throughout the alloy [29].

Figure 36 shows **that the size of intermetallic in Al-15Ce alloy has reduced with adding element.**

The average grain size of the Al-15Ce alloy was measured to be 278.68 μm, which was reduced to 197.17 μm and 33.42 μm with the addition of magnesium and scandium-zirconium, respectively, as shown in **Figure 35**. SEM image shown in **Figure 36** reveal that the size of intermetallic in Al-15Ce alloy has reduced with adding element. The average intermetallic size of the Al-15Ce was also reduced from 22.21 μm to 22.17 μm and 20.17 μm with the addition of magnesium and scandium-zirconium, respectively, as shown in **Figure 32**, indicating a refinement of the microstructure. However, the percentage area of intermetallic increased from 15.77% in the Al-15Ce alloy to 19.876% and 20.44% with the addition of magnesium and scandium-zirconium, respectively, as shown in **Figure 29**. These results suggest that adding magnesium and scandium-zirconium can improve the microstructure of Al-15Ce.

The addition of magnesium (Mg), scandium (Sc), and zirconium (Zr) to Al-15Ce alloys can have a significant effect on their microstructure and properties. When magnesium is added to Al-15Ce alloys, it can react with the cerium to form $Al_{11}Ce_3$ intermetallic particles [14]. When scandium and zirconium are added to Al-15Ce alloys, they can react to form Al_3(Sc, Zr) intermetallic particles [7]. These particles can act as heterogeneous nucleation sites for forming the aluminum-rich solid solution, which can refine the grain structure and form smaller, more uniformly distributed grains [7].

4.3 Effect of Mg, Sc, and Zr on phase formation in Al-15Ce alloys

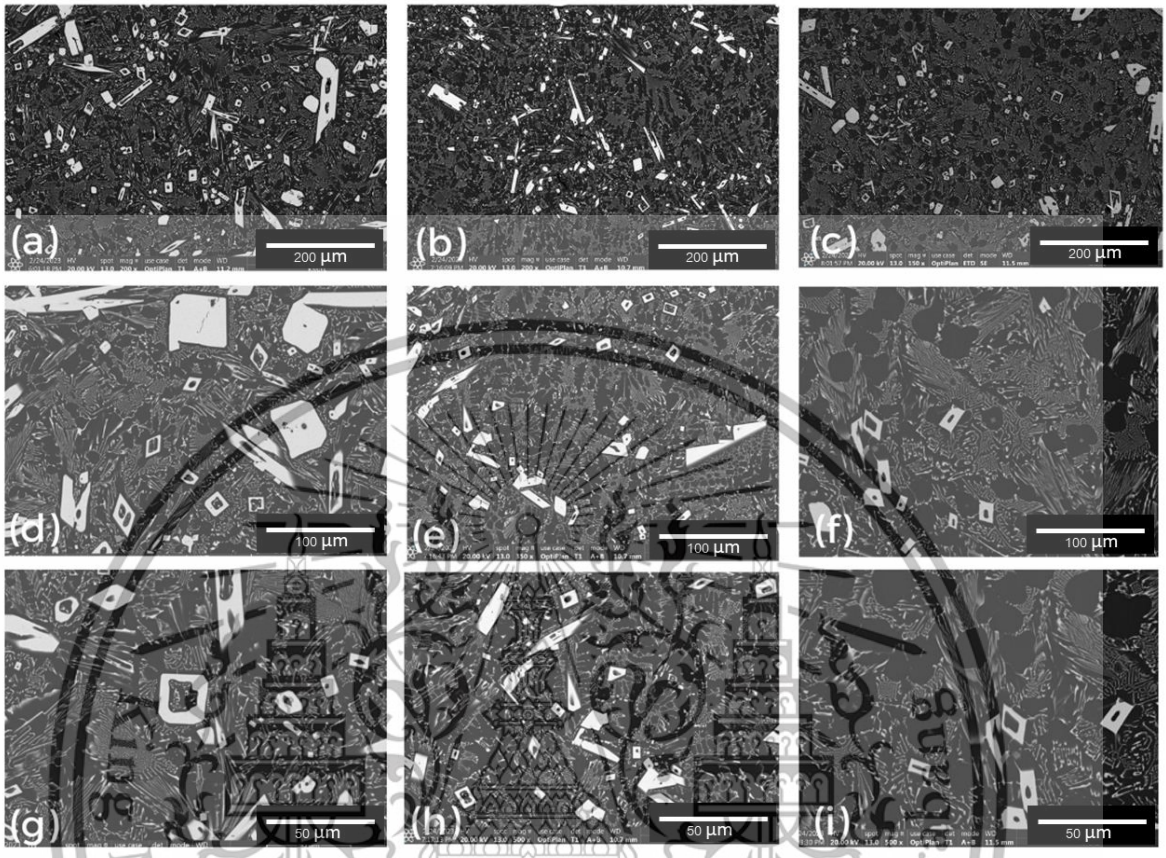

Figure 36 SEM image of as-cast (a, d, g) Al-15Ce, (b, e, h) Al-15Ce-0.75Mg and (c, f, i) Al-15Ce -0.75Mg-0.2Sc-0.2Zr alloys with low cooling rate.

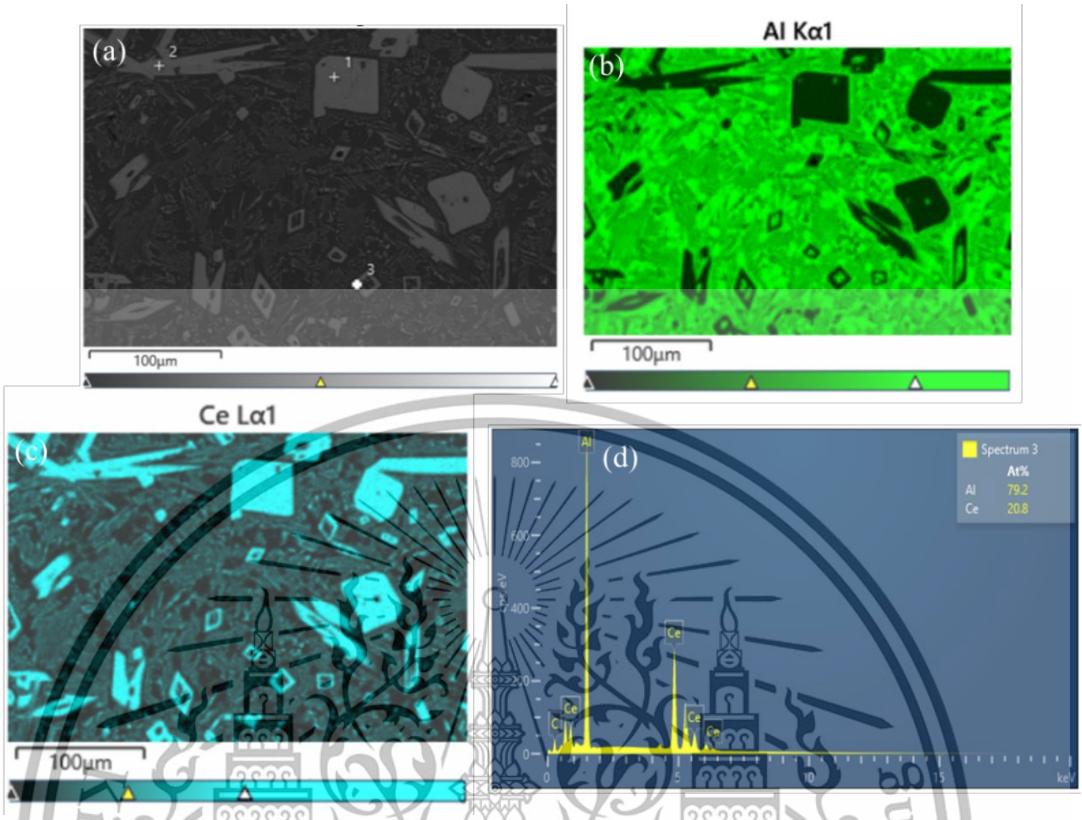

Figure 37 (a) SEM image of Al-15Ce alloys, (b) Al, (c) Ce and (d) EDS mapping.

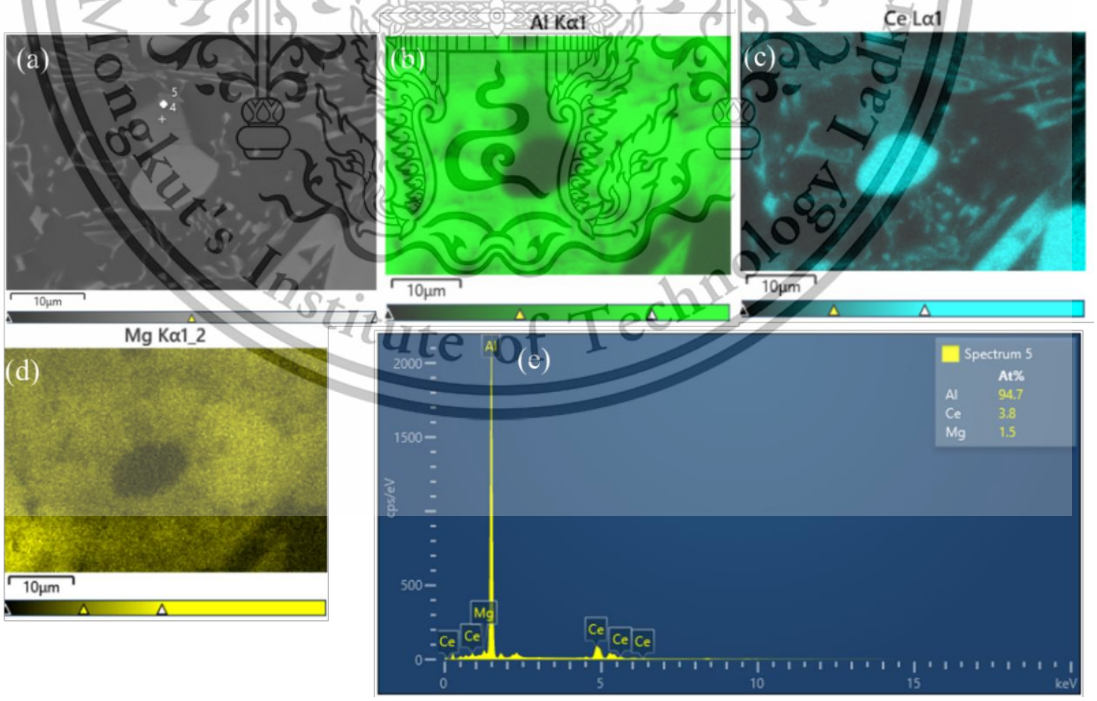

Figure 38 (a) SEM image of Al-15Ce-075Mg alloys, (b) Al, (c) Ce, (d) Mg and (e) EDS mapping.

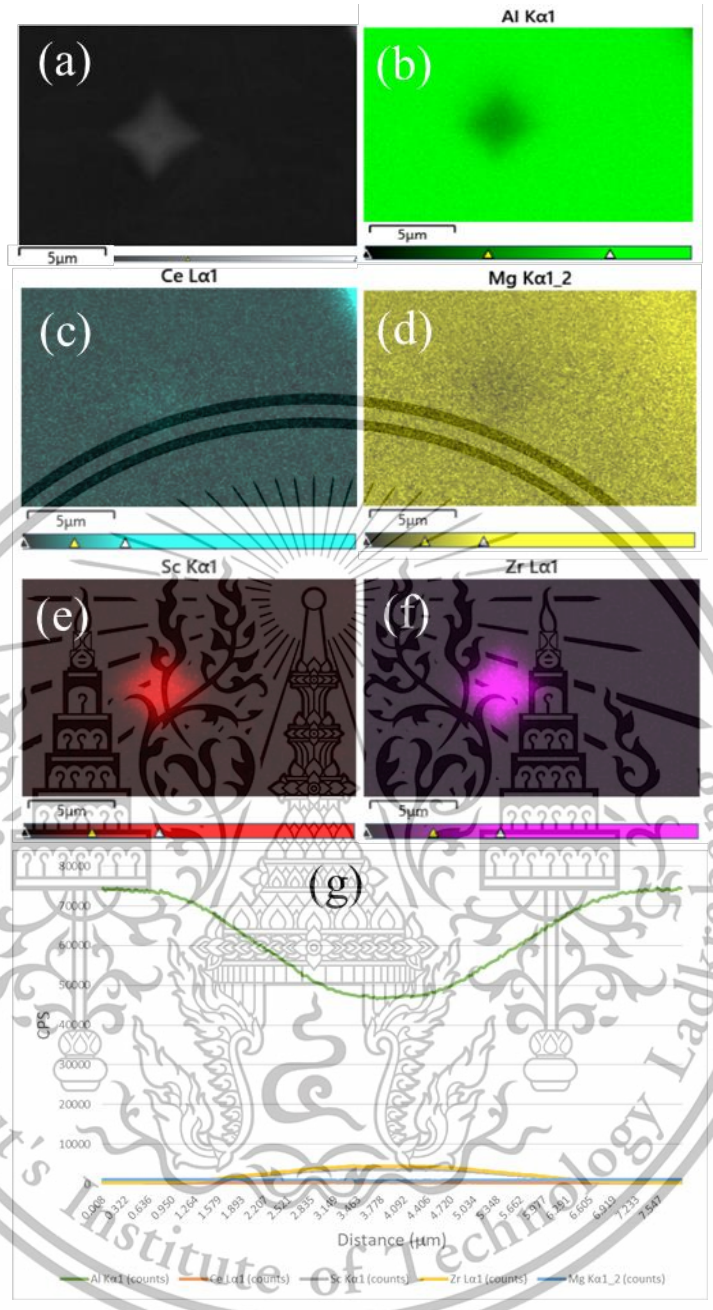

Figure 39 (a) SEM image of Al-15Ce-075Mg-0.2Sc-0.2Zr alloy, (b) Al, (c) Ce, (d) Mg, (e) Sc, (f) Zr and (e) EDS line scan across through the Al3(Sc, Zr) phase.

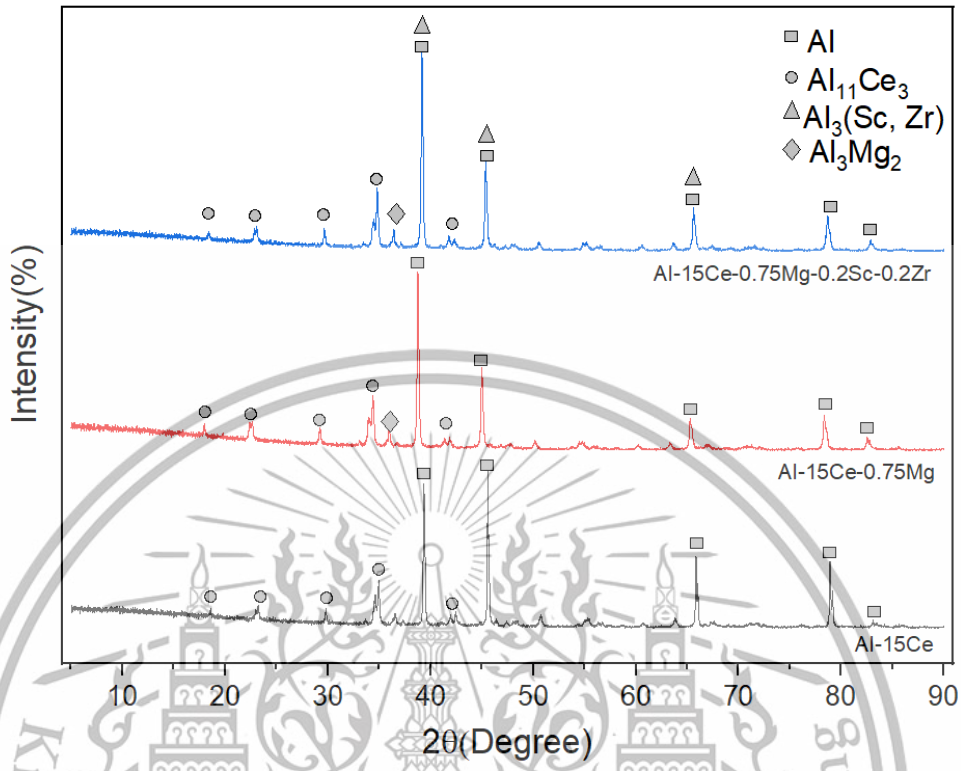

Figure 40 XRD Pattern of as-cast Al-15Ce, Al-15Ce-0.75Mg, and Al-15Ce-0.75Mg-0.2Sc-0.2Zr alloys with low cooling rate.

The SEM image of the EDS map of the alloy is presented—the intermetallic compounds of Al-15Ce alloys, as shown in **Figure 37**. The result reveals the presence of Al and Ce phases. The alloy is expected to be found $Al_{11}Ce_3$ phase. The intermetallic compounds of Al-15Ce-0.75mg alloys as shown in **Figure 38.** The result reveals the presence of Al, Ce, and Mg phases. The alloy is expected to find the Al_3Mg_2 phase. The intermetallic compounds of Al-15Ce -0.75Mg-0.2Sc-0.2Zr alloys as shown in **Figure 39**; The result reveals the presence of Al, Sc, and Zr phases. The alloy is expected to be found Al_3(Sc, Zr) phase. The XRD patterns shown in **Figure 40** indicate the same result.

4.4 Mechanical properties of Al-15Ce

4.4.1 Effect of different cooling rate on Al-15Ce hardness

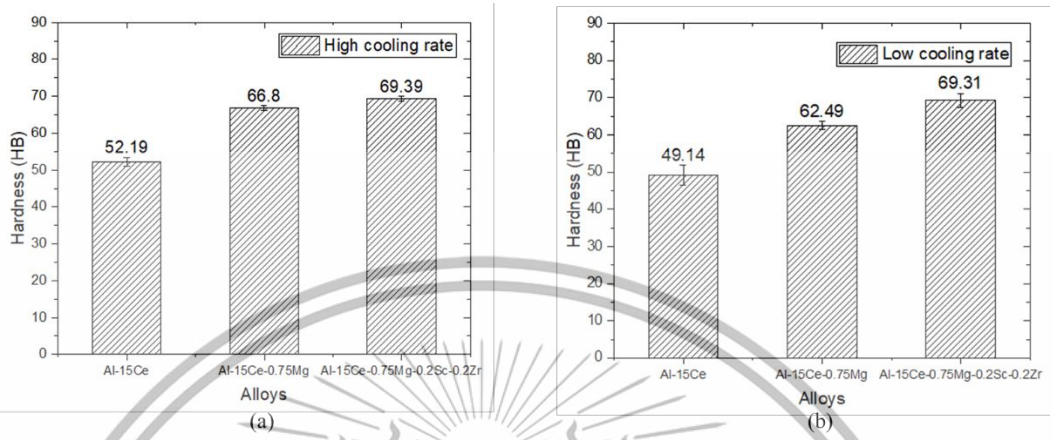

Figure 41 Average of hardness of as-cast Al-15Ce, Al-15Ce-0.75Mg, and Al-15Ce-0.75Mg-0.2Sc-0.2Zr alloys with (a) high cooling rate, (b) low cooling rate.

According to the hardness test results of aluminum alloy Al-15Ce, Al-15Ce-0.75Mg, and Al-15Ce-0.75Mg-0.2Sc-0.2Zr, as shown in **Figure 41**. When considering the hardness of workpieces with different cooling rates from Figure 40, it was found that the high cooling rate of Al-15Ce has no significant change in hardness value compared with the low cooling rate workpiece. The high cooling rate of Al-15Ce alloy with the addition of Mg, Sc, Zr has a slight increase in hardness value compared with the low cooling rate workpiece.

The cooling rate during the solidification process impacts the hardness of Al-15Ce alloys. Generally, a high cooling rate leads to a higher hardness due to forming of a finer microstructure and a more homogeneous distribution of strengthening phases [30]. When Al-15Ce alloys are slowly cooled, the intermetallic compounds can grow larger and coarsen, resulting in larger grain sizes and less uniform distribution of the strengthening phases. This can lead to decreasing the hardness of the alloy. [30].

On the other hand, when Al-15Ce alloys are rapidly cooled, the solidification process occurs more quickly, and the intermetallic compounds have less time to grow and coarsen. As a result, the alloy can have a finer microstructure with a more uniform distribution of the strengthening phases [30]. This can increase hardness due to the increased number of intermetallic compounds and their distribution in the aluminum matrix.

4.4.2 Effect of adding element on Al-15Ce hardness

The impact of adding elements on the hardness of Al-15Ce alloys was investigated by conducting hardness tests on Al-15Ce, Al-15Ce-0.75Mg, and Al-15Ce-0.75Mg-0.2Sc-0.2Zr alloys. Analysis of the results from **Figure 41** reveals that adding 0.75 wt.% magnesium increased the hardness value from 52.19 HB to 66.80 HB. However, adding 0.2 wt.% zirconium and scandium increased the hardness value to 69.39 HB. These results suggest that the inclusion of magnesium, zirconium, and scandium substantially impacts the hardness of Al-15Ce alloys.

The strengthening effect of magnesium is further enhanced by the interaction with the intermetallic compounds in the alloy. For example, magnesium can react with Ce-rich intermetallic compounds to form new phases, which can act as additional hardening agents [14]. When scandium is added to Al-15Ce alloys, it forms intermetallic compounds such as Al_3(Sc, Zr), which can act as hardening agents due to their high melting points and strength. The formation of these intermetallic compounds can also refine the grain structure of the alloy, leading to an increase in its strength and hardness [15].

Overall, adding magnesium to Al-15Ce alloys can increase their hardness due to the solid solution strengthening effect and the formation of new strengthening phases. The precise increase in hardness depends on several factors, including the amount of element added, the aging temperature and time, and the cooling rate during solidification.

4.4.3 Hardness after aging at different temperatures

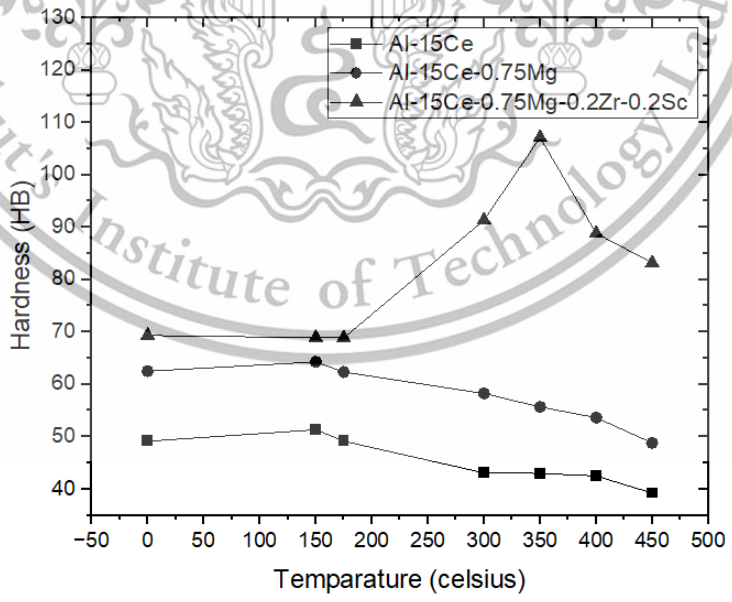

Figure 42 Hardness evolution during isothermal aging for 3 hours at different temperatures of Al-15Ce, Al-15Ce-0.75Mg, and Al-15Ce-0.75Mg-0.2Sc-0.2Zr alloys.

The microhardness of aluminum alloys with different additives can be significantly affected by the heat exposure temperature. This study analyzed a graph of the microhardness of various aluminum-cerium alloys with different additives after heat exposure at different temperatures. The results in **Figure 42** showed that adding magnesium to aluminum-cerium alloys resulted in the highest microhardness at 150 °C to 175 °C, while the addition of scandium and zirconium resulted in the highest microhardness at 350 °C. As a result, this study aims to conduct a thermal exposure experiment at 150 °C, 175 °C, and 350 °C to investigate further the effects of heat exposure on the microhardness of aluminum-cerium alloys with different alloying element addition.

4.4.4 Effect of alloys element on aging at different temperature and cooling rate in as-cast stage

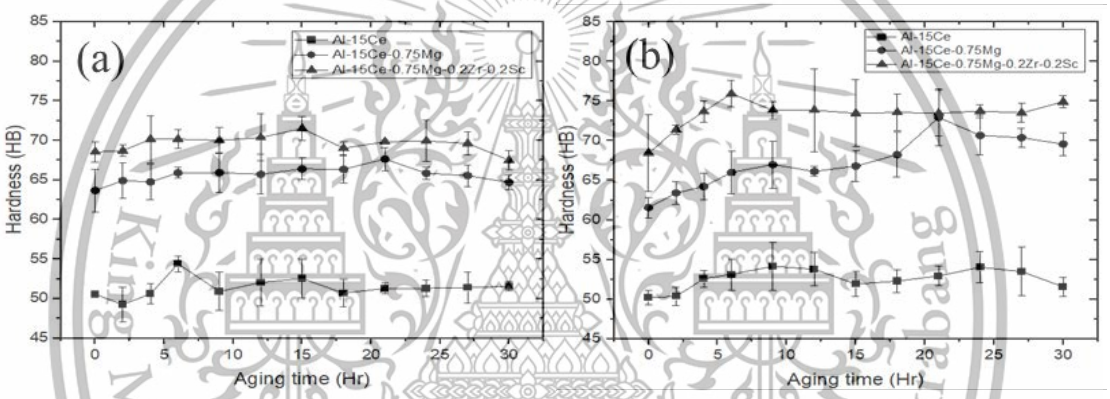

Figure 43 Hardness evolution during isothermal aging at 150 ºC of Al-15Ce, Al-15Ce-0.75Mg, and Al-15Ce-0.75Mg-0.2Sc-0.2Zr alloys with different condition (a) high cooling rate, (b) low cooling rate.

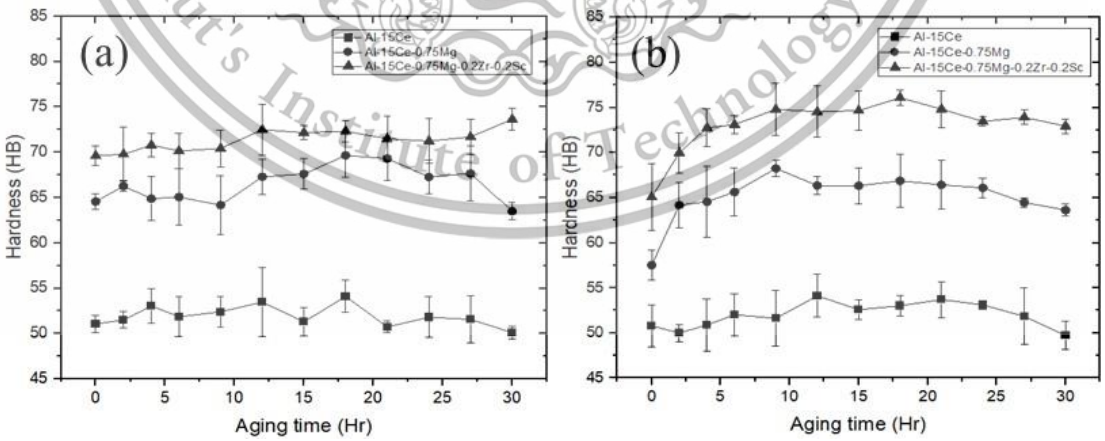

Figure 44 Hardness evolution during isothermal aging at 175 ºC of Al-15Ce, Al-15Ce-0.75Mg, and Al-15Ce-0.75Mg-0.2Sc-0.2Zr alloys with different condition (a) high cooling rate, (b) low cooling rate.

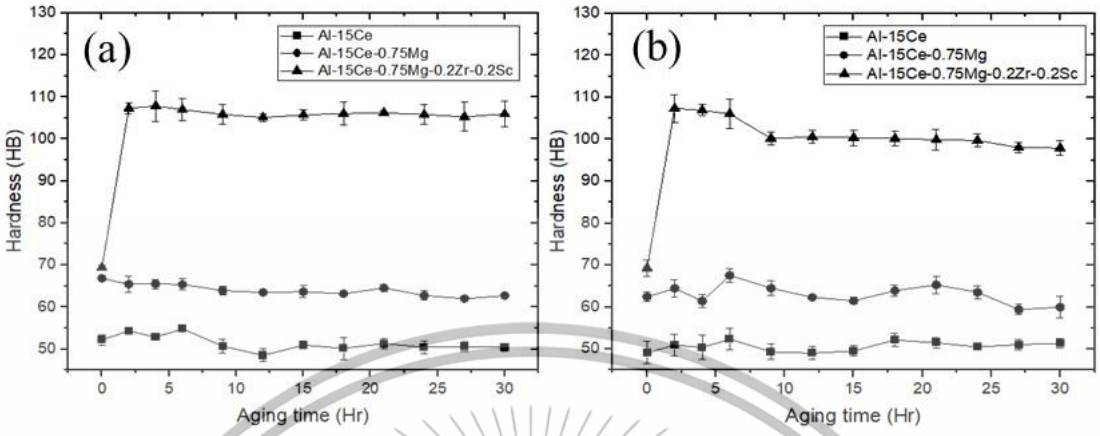

Figure 45 Hardness evolution during isothermal aging at 350 ºC of Al-15Ce, Al-15Ce-0.75Mg, and Al-15Ce-0.75Mg-0.2Sc-0.2Zr alloys with different condition (a) high cooling rate, (b) low cooling rate.

Figure 43, Figure 44, and **Figure 45** presented in this study depict the microhardness evolution of three different alloys under isothermal aging at 150 °C, 175 °C, and 350 °C for up to 30 hours. The Al-15Ce alloy displayed insignificant changes in microhardness after the aging process, with a value of approximately 52 HB, as shown in **Figure 43**. In contrast, the Al-15Ce-0.75Mg alloy showed a slight increase in hardness at 150 °C and 175 °C, reaching a maximum value of 72 HB and 69 HB, as shown in **Figure 44**, respectively. However, at 350 °C, the hardness remained relatively constant, peaking at around 65 HB, as shown in **Figure 45**.

Similarly, the Al-15Ce-0.75Mg-0.2Sc-0.2Zr alloy exhibited a slight increase in microhardness after heat treatment at 150 °C and 175 °C, with a peak value of around 74 HB, as shown in **Figure 45**. However, at 350 °C, the microhardness increased rapidly to a peak of 107 HB after 2 hours of exposure before gradually decreasing after 8 hours. Subsequently, the microhardness remained constant, as shown in **Figure 45**.

In summary, In Al-Ce alloys, precipitation hardening is the primary mechanism for increasing hardness during aging. Adding magnesium promotes the formation of strengthening precipitates of $Al_{11}Ce_3$, within the aluminum matrix during aging. These precipitates act as obstacles to dislocation movement, increasing hardness and strength [14].

Adding magnesium can accelerate the precipitation kinetics of cerium-containing phases in the alloy. Magnesium atoms act as nucleation sites for the formation of precipitates, providing additional sites for the cerium atoms to segregate and form strengthening phases. This enhanced precipitation kinetics results in a higher density and finer distribution of precipitates, contributing to increased hardness. Likewise, Adding Sc and Zr promotes the formation of strengthening precipitates, such as Al_3(Sc, Zr), within the aluminum matrix

during aging. This precipitate also helps increase the hardness of the alloy during the aging process [31].

4.4.5 Effect of aging temperature in the alloys at different cooling rate in as-cast stage

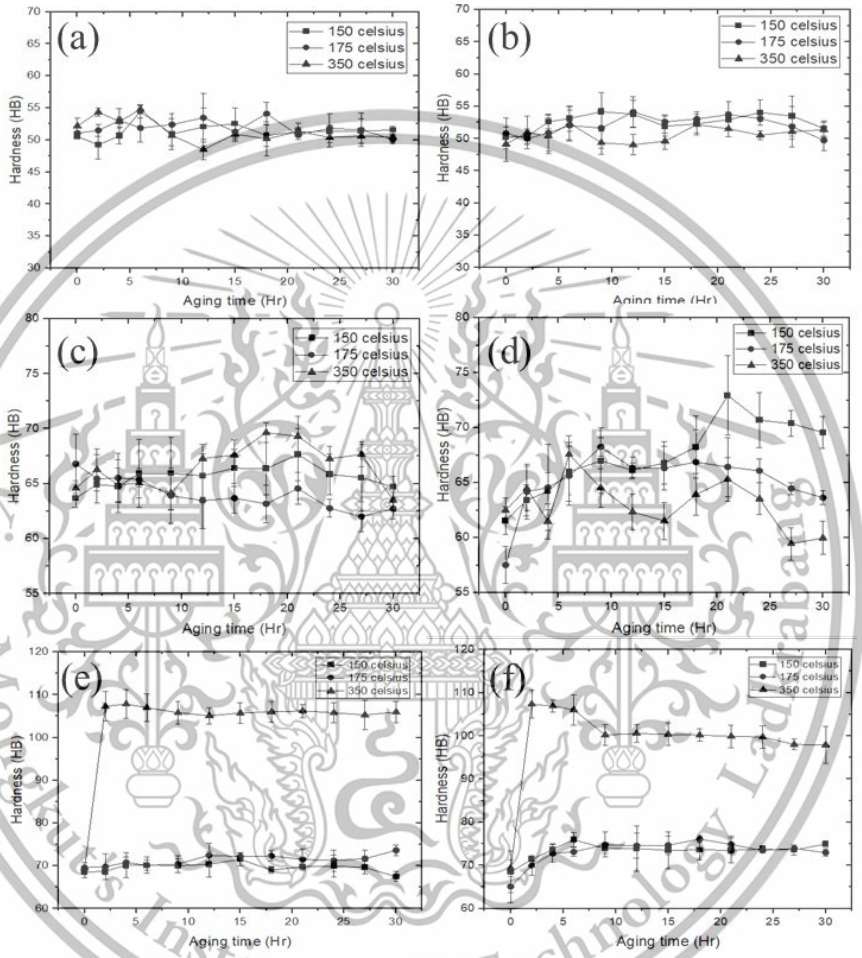

Figure 46 Hardness evolution during different isothermal aging temperatures of (a, b) Al-15Ce, (c, d) Al-15Ce-0.75Mg and (e, f) Al-15Ce-0.75Mg-0.2Sc-0.2Zr alloy with different conditions (a, c, e) high cooling rate, (b, d, f) low cooling rate.

As shown in **Figure 46 (a, b)**, For Al-15Ce alloy, the hardness has no significant difference between the three aging temperatures. For Al-15Ce-0.75Mg, the hardness when aging with 150 has slightly higher than the other temperatures, as shown in **Figure 46 (c, d).** Al-15Ce-0.75Mg-0.2Sc-0.2Zr, with an aging temperature of 350, has the highest hardness compared to the different aging temperatures, as shown in **Figure 46 (e, f)**.

It can be concluded that the Al-15Ce-0.75Mg alloy displayed the highest microhardness when aged at 150 °C, whereas the Al-15Ce-0.75Mg-0.2Sc-0.2Zr alloy exhibited the highest microhardness when aged at 350 °C.

The aging temperature and cooling rate play significant roles in determining alloys' microstructure and properties in the as-cast stage. The choice of aging temperature affects the rate of precipitation and the formation of desired strengthening phases in the material. Different alloying elements have specific solubilities and diffusion rates at different temperatures. The appropriate aging temperature allows for the optimal kinetics of precipitation, ensuring the formation of fine and evenly distributed precipitates within the material [32].

4.4.5 Tensile test

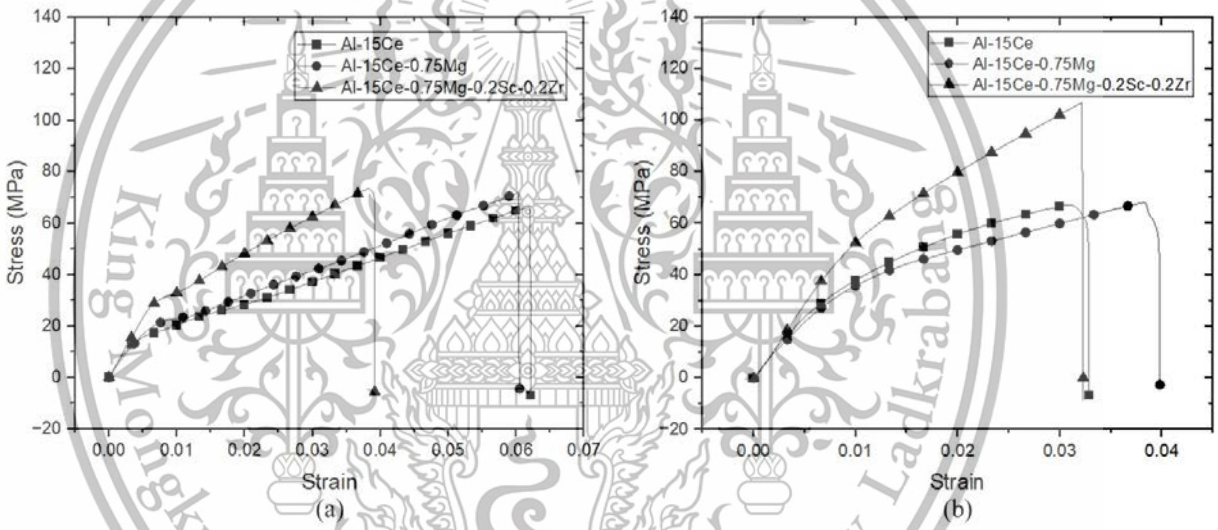

Figure 47 Representative stress versus strain curves for Al-15Ce, Al-15Ce-0.75Mg, and Al-15Ce-0.75Mg-0.2Sc-0.2Zr alloys with aging at (a) 150 ºC and (b) 350 ºC.

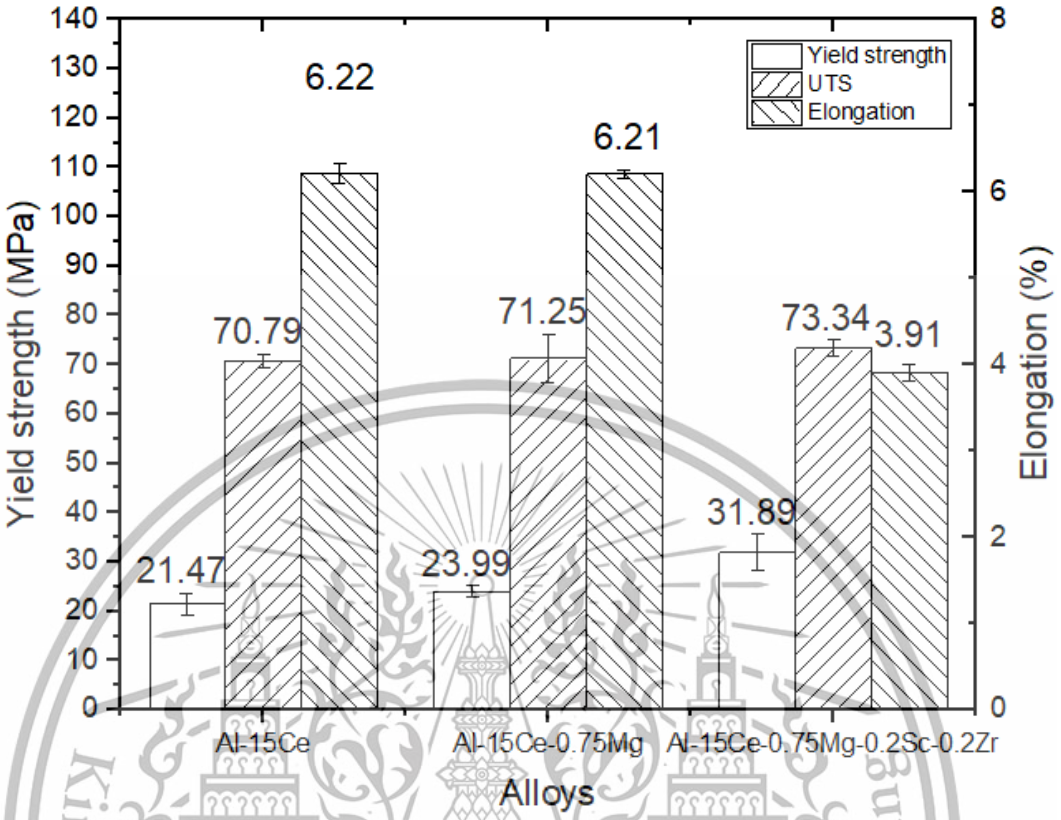

Figure 48 Mechanical properties of Al-15Ce, Al-15Ce-0.75Mg, and Al-15Ce-0.75Mg-0.2Sc-0.2Zr alloys with aging at 150 °C.

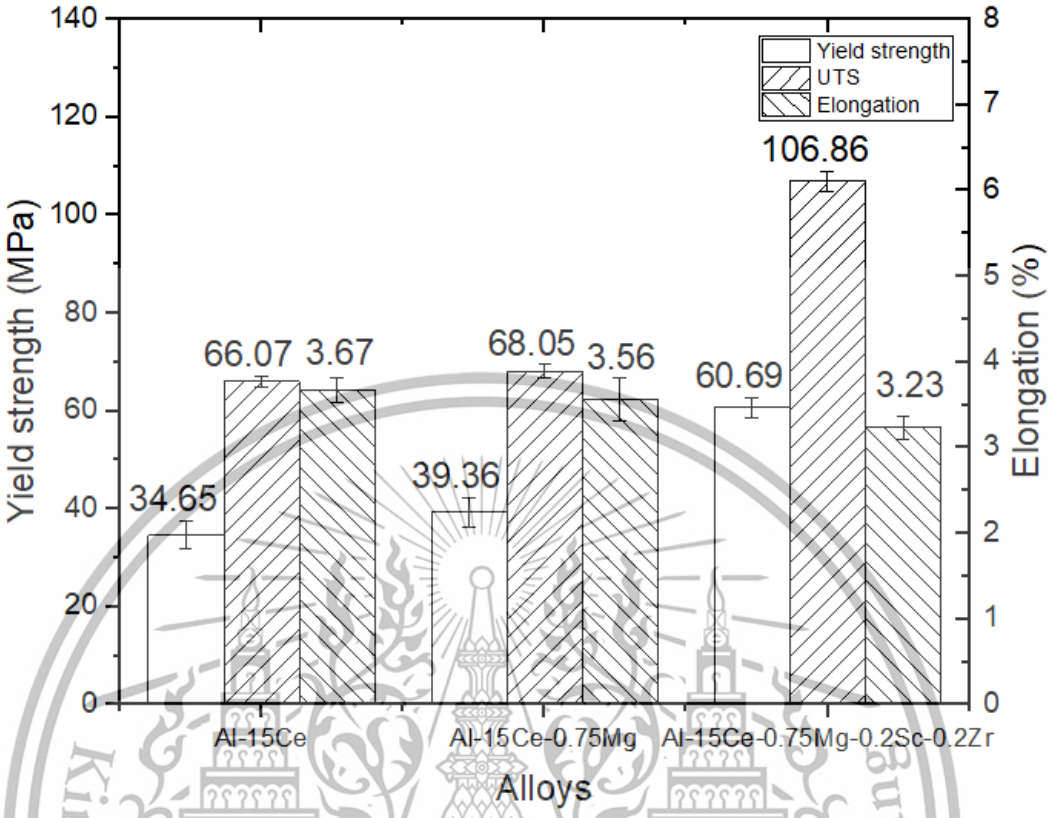

Figure 49 Mechanical properties of Al-15Ce, Al-15Ce-0.75Mg, and Al-15Ce-0.75Mg-0.2Sc-0.2Zr alloys with aging at 350 ºC.

The stress-strain curve at room temperature with aging at 150 °C and 350 °C are shown in **Figure 47.** The mechanical properties of Al-15Ce, Al-15Ce-0.75Mg and Al-15Ce-0.75Mg-0.2Sc-0.2Zr are summarized in **Figure 48** and **Figure 49**. Additions of Magnesium in Al-15Ce alloys with aging 150 °C, cause to increase yield strength of alloys from 21.47 to 23.99 MPa and ultimate tensile strength increase from 70.79 to 71.25 MPa in **Figure 48**. Additions of Magnesium, Zirconium and Scandium in Al-15Ce alloys, cause to increase in yield strength of alloys from 21.47 to 31.89 MPa and ultimate tensile strength increase from 70.79 to 73.34 MPa in **Figure 48**. However, there was a significant lowering elongation of alloys from 6.22 to 6.21 pct in terms of addition Magnesium and 6.22 to 3.91 pct in terms of addition magnesium, Zirconium and Scandium **Figure 48.**

Additions of Magnesium in Al-15Ce alloys with aging 350 °C, cause to increase yield strength of alloys from 34.65 to 39.36 MPa and ultimate tensile strength increase from 66.07 to 68.05 MPa in **Figure 49**. Additions of Magnesium, Zirconium and Scandium in Al-15Ce alloys, cause to increase in yield strength of alloys from 34.65 to 60.69 MPa and ultimate tensile strength increase from 66.07 to 106.86 MPa in **Figure 49**. However, there was a significant lowering elongation of alloys from 3.67 to 3.56 pct in terms of addition Magnesium and 3.67 to 3.23 pct in terms of addition Magnesium, Zirconium and Scandium **Figure 49.**

The result of mechanical properties can conclude that addition of Magnesium, Zirconium and Scandium causes to increase yield strength and ultimate tensile strength. mechanical properties of Al-15Ce-0.75Mg-0.2Sc-0.2Zr with aging 350 °C is better strength than aging 150 °C. Conversely, Al-15Ce and Al-15Ce-0.75Mg with aging 350 °C are lower strength than aging 150 °C. Therefore, it can be concluded that Al-15Ce-0.75Mg-0.2Sc-0.2Zr with aging 350 °C remarkable potential in mechanical properties.

4.4.6 Fracture analysis

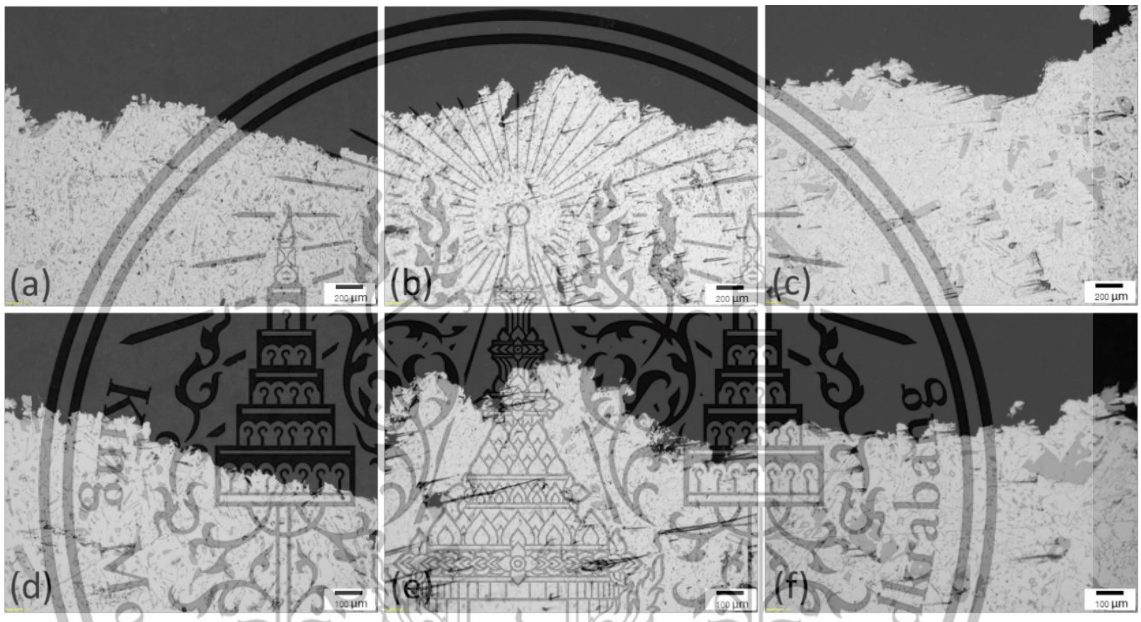

Figure 50 Tensile fracture morphology of the (a, d) Al-15Ce, (b, e) Al-15Ce-0.75Mg, and (c, f) Al-15Ce-0.75Mg-0.2Sc-0.2Zr alloys with aging at 150 ºC and different magnificent (a, b, c) 200 μm (d, e, f) 100 μm.

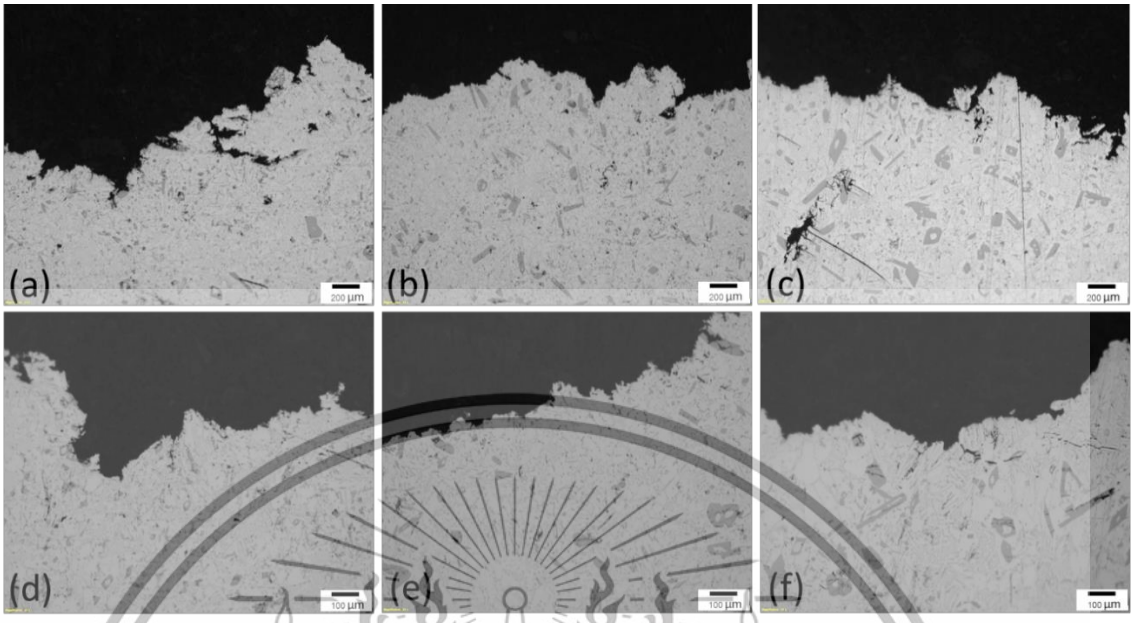

Figure 51 Tensile fracture morphology of the (a, d) Al-15Ce, (b, e) Al-15Ce-0.75Mg, and (c, f) Al-15Ce-0.75Mg-0.2Sc-0.2Zr alloys with aging at 350 ºC and different magnificent (a, b, c) 200 μm (d, e, f) 100 μm.

The fracture morphology of the alloys after heat treatment for different temperatures is illustrated in **Figure 50** and **Figure 51**. When a tensile fracture occurs in intermetallic compounds, it is often characterized by a low number of measurable tensile values. Intermetallic compounds generally exhibit brittle behavior, which means they have limited ability to undergo plastic deformation before fracture. As a result, the tensile fracture may happen at relatively low levels of applied stress or strain.

CHAPTER 5 SUMMARY OF EXPERIMENT RESULTS AND RECOMMENDATIONS

An overview of the results of experiments is provided in this chapter, along with recommendations based on research on the creation of the metals cerium aluminum by adding the elements magnesium, zirconium, and scandium, as well as the cooling rate that impacts the mechanical properties. and microstructure, as in the following topics.

5.1 Conclusion

1. The microstructure of Aluminum Cerium alloy mainly consists of unevenly distributed intermetallic compounds and a eutectic phase. The SEM and XRD analysis of Al-15Ce alloys reveals the presence of the $Al_{11}Ce_3$, Al_3Mg_2, and Al_3(Sc, Zr) phases.
2. The cooling rate affects the size and distribution of intermetallic particles in Al-15Ce alloys. Slow cooling results in larger particles, while rapid cooling results in smaller particles that enhance these properties.
3. Adding magnesium and scandium-zirconium can improve the microstructure of Al-15Ce by refining the grain structure and reducing intermetallic size but increasing the percentage area of intermetallic.
4. The cooling rate affects the hardness of Al-15Ce alloys, with high cooling rates resulting in a finer microstructure and a more homogeneous distribution of strengthening phases, leading to higher hardness. Slow cooling can result in larger grain sizes and less uniform distribution of strengthening phases, leading to decreased hardness.
5. The hardness can be improved by aging at 150 °C for Al-15Ce-0.75Mg and at 350 °C for Al-15Ce-0.75Mg-0.2Sc-0.2Zr. The maximum hardness of Al-15Ce-0.75Mg alloy can be reached after aging at 150 °C up to 72 HB while adding Sc, Zr to the alloy can improve the hardness up to 107 HB after aging at 350 °C for 30 hours.
6. Adding Magnesium, Zirconium, and Scandium in Al-15Ce alloys increases yield strength and ultimate tensile strength. Al-15Ce-0.75Mg-0.2Sc-0.2Zr with aging at 350 °C shows remarkable potential in mechanical properties compared to Al-15Ce and Al-15Ce-0.75Mg with aging at 150 °C.
7. Intermetallic compounds exhibit brittle behavior and have limited ability to undergo plastic deformation before fracture, resulting in low measurable tensile values at relatively low levels of applied stress or strain.

5.2 Recommendation

The subject of this thesis is the development of an aluminum cerium alloy by adding elements to enhance microstructure and improve mechanical qualities, including hardness and strength. If you desire to develop an aluminum alloy that can match the demands of the current industry. In that case, the impact on microstructure, mechanical characteristics, electrical conductivity, and corrosion resistance must be considered.

Our group suggests that future work could investigate the effect of different aging temperatures and times on Aluminum Cerium alloys' microstructure and mechanical properties. It will be more beneficial to our work if we can minimize the casting faults. Testing currently available specimens from neighboring specimen locations with few casting flaws could assist in more precise conclusions.

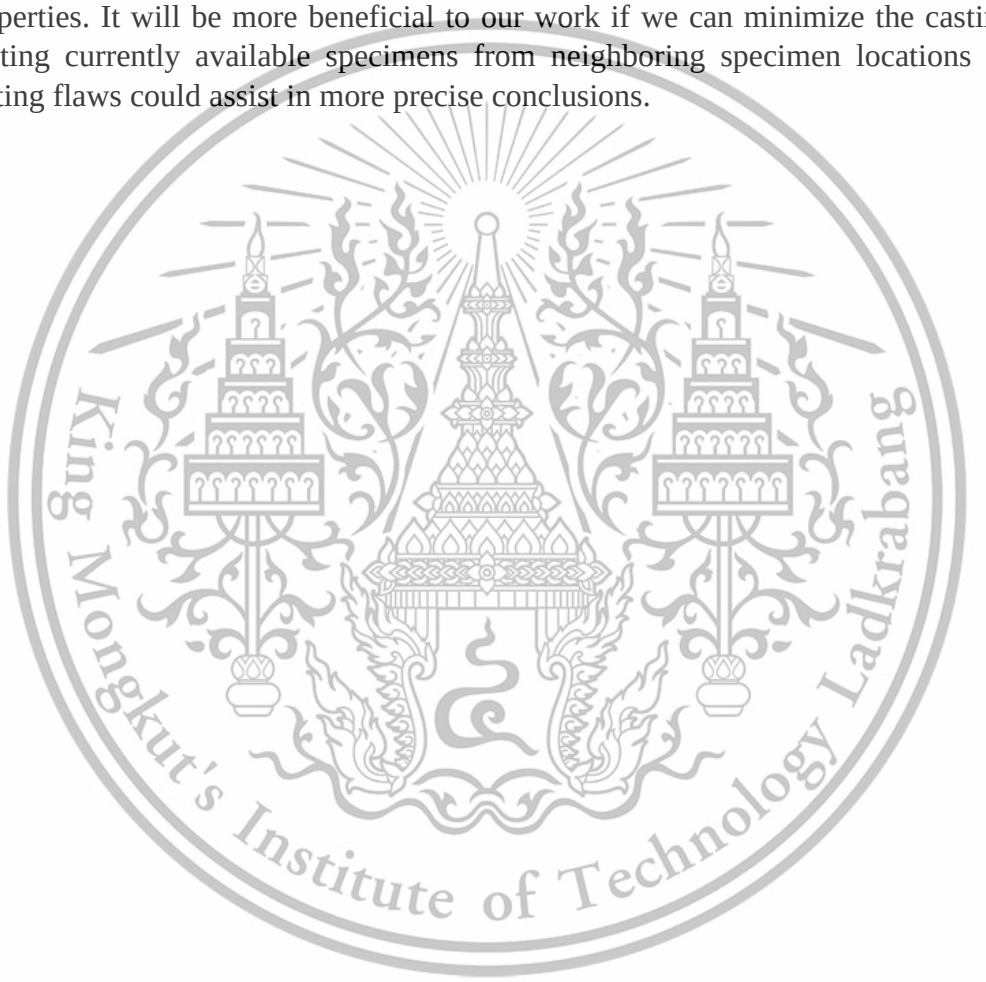

Reference

1. Czerwinski, F. (1970) *Cerium in aluminum alloys*, *AGRIS*. Available at: https://agris.fao.org/agris-search/search.do?recordID=US202000023874 (Accessed: 20 May 2023).
2. Sims, Z.C. *et al.* (2017) *High performance aluminum–cerium alloys for high-temperature applications*, *Materials Horizons*. Available at: https://www.osti.gov/pages/biblio/1409366 (Accessed: 20 May 2023).
3. Zhang, L., Eskin, D.G. and Katgerman, L. (2011) *Influence of ultrasonic melt treatment on the formation of primary intermetallics and related grain refinement in aluminum alloys*, *SpringerLink*. Available at: https://link.springer.com/article/10.1007/s10853-011-5463-2 (Accessed: 20 May 2023).
4. *Age hardening aluminum - aluminum age hardening* (no date) *ThermTech*. Available at: https://www.thermtech.net/heat-treating-services/hardening/age-hardening.php#:~:text=Process%20of%20Age%20Hardening,hours%20depending%20on%20the%20material (Accessed: 20 May 2023).
5. *Artificial ageing* (no date) *Artificial Ageing - an overview | ScienceDirect Topics*. Available at: https://www.sciencedirect.com/topics/engineering/artificial-ageing (Accessed: 20 May 2023).
6. *Effect of alloying elements on thermal stability of aluminium-cerium based alloys* (2022) *Home*. Available at: https://www.researchsquare.com/article/rs-67587/v3 (Accessed: 20 May 2023).
7. Author links open overlay panelLiyang Wang *et al.* (2021) *Effect of zr and SC micro-additions on the microstructure and mechanical properties of AS-cast al-5ce alloy*, *Materials Science and Engineering: A*. Available at: https://www.sciencedirect.com/science/article/abs/pii/S0921509321009229 (Accessed: 20 May 2023).
8. G. Chen, Z. Zhang, L. Chen, et al. (2019). Microstructures and mechanical properties of Al-Ce alloys. Journal of Alloys and Compounds, 797, 992-1002. (Accessed: 20 May 2023)
9. M.A. Kumar, B. Srinivasarao, V.V. Bhanu Prasad, et al. (2019). Effect of cerium addition on the microstructure and mechanical properties of Al–Mg alloy. Journal of Materials Research and Technology, 8(1), 1063-1074. (Accessed: 20 May 2023)
10. A.K. Lakshmi, R. Rathish Kumar, S. Kumar, et al. (2017). Microstructure and mechanical properties of Al-Ce alloy processed by equal channel angular pressing. Journal of Materials Science, 52(1), 175-187. (Accessed: 20 May 2023)
11. Indicated (no date) *Casting Process*, *Casting process*. Available at: https://www.summaryplanet.com/engineering/Casting-Process.html (Accessed: 20 May 2023).
12. Author links open overlay panelDaniel S. Ng 1 *et al.* (2020) *Aging- and creep-resistance of a cast hypoeutectic al-6.9ce-9.3mg (wt.%) alloy*, *Materials Science and Engineering: A*. Available at: https://www.sciencedirect.com/science/article/abs/pii/S0921509320304792 (Accessed: 20 May 2023).
13. Author links open overlay panelBo Hu a *et al.* (2021) *Solid solution strengthening mechanism in high pressure die casting Al–Ce–mg alloys*, *Materials Science and Engineering: A*. Available at:

https://www.sciencedirect.com/science/article/abs/pii/S0921509321003786 (Accessed: 20 May 2023).

14. (2022) *Effect of alloying elements on thermal stability of Aluminium-Cerium based alloys*. Available at: https://assets.researchsquare.com/files/rs-67587/v3_covered.pdf?c=1648657619 (Accessed: 20 May 2023).
15. Author links open overlay panelJieyun Ye a b *et al.* (2022) *Beneficial effects of SC/ZR addition on hypereutectic Al–CE alloys: Modification of primary phases and precipitation hardening, Materials Science and Engineering: A*. Available at: https://www.sciencedirect.com/science/article/abs/pii/S0921509322000193 (Accessed: 20 May 2023).
16. Author links open overlay panelJovid U. Rakhmonov a *et al.* (2022) *Comparing evolution of precipitates and strength upon aging of cast and laser-remelted al–8ce-0.2sc-0.1zr (wt.%), Materials Science and Engineering: A*. Available at: https://www.sciencedirect.com/science/article/abs/pii/S0921509322003975 (Accessed: 20 May 2023).
17. Zhang, L., & Duan, H. (2019). Advances in ultrasonic treatment of molten metals and alloys: A review. Ultrasonics Sonochemistry, 56, 208-227. (Accessed: 20 May 2023).
18. Sklyar, V., Yaskiv, O., Zinigrad, M., & Dirker, J. (2018). Ultrasonic cavitation processing: A review. Ultrasonics Sonochemistry, 40, 770-782. (Accessed: 20 May 2023).
19. Zhang, L., Eskin, D.G. and Katgerman, L. (2011) *Influence of ultrasonic melt treatment on the formation of primary intermetallics and related grain refinement in aluminum alloys - journal of materials science, SpringerLink*. Available at: https://link.springer.com/article/10.1007/s10853-011-5463-2 (Accessed: 20 May 2023).
20. Precipitation hardening of aluminum alloys (2020) Precipitation Hardening of Aluminum Alloys: Total Materia Article. Available at: https://www.totalmateria.com/page.aspx?ID=CheckArticle&site=ktn&NM=235 (Accessed: 20 May 2023).
21. Aluminum extraction (2015) Aluminum Extraction - an overview | ScienceDirect Topics. Available at: https://www.sciencedirect.com/topics/materials-science/aluminum-extraction (Accessed: 20 May 2023).
22. (No date) *Beneficial effects of SC/ZR addition on hypereutectic Al–CE alloys* ... Available at: https://www.researchgate.net/publication/357614831_Beneficial_effects_of_ScZr_addition_on_hypereutectic_Al-Ce_alloys_Modification_of_primary_phases_and_precipitation_hardening (Accessed: 20 May 2023).
23. *Brinell - determine the hardness of different materials* (no date) *Brinell - Determine the hardness of different materials*. Available at: https://rime.de/en/wiki/brinell-hardness-test/ (Accessed: 20 May 2023).
24. *Brinell hardness test* (2022) *Nuclear Power*. Available at: https://www.nuclear-power.com/nuclear-engineering/materials-science/material-properties/hardness/brinell-hardness-test/ (Accessed: 20 May 2023).
25. *Tensile strength tester* (no date) *Astro Instrument Co., Ltd.* Available at: https://www.astroinstrument.com/knowledge/tensile-strength-tester/ (Accessed: 20 May 2023).

26. *Home* (no date) *TestResources*. Available at: https://www.testresources.net/applications/test-types/tensile-test/ (Accessed: 20 May 2023).
27. byCSWIP, P. (no date) *Mechanical testing - tensile test, CSWIP Questions - CQ*. Available at: http://cswipquestions.blogspot.com/2014/08/mechanical-testing-tensile-test.html (Accessed: 20 May 2023).
28. Author links open overlay panelHo Sung Jang a b *et al.* (2022) *Effect of ultrasonic melt treatment conditions on melt quality of al–mg alloy, Journal of Materials Research and Technology*. Available at: https://www.sciencedirect.com/science/article/pii/S2238785422009000 (Accessed: 25 May 2023).
29. (No date) *Effect of cooling rate on microstructure and properties of twin-roll ...* Available at: https://mdpi-res.com/d_attachment/metals/metals-10-01168/article_deploy/metals-10-01168.pdf (Accessed: 24 May 2023).
30. Author links open overlay panelHua-Ping Tang a *et al.* (2019) *Effect of cooling rate on microstructure and mechanical properties of an al-5.0mg-3.0zn-1.0cu cast alloy, Journal of Alloys and Compounds*. Available at: https://www.sciencedirect.com/science/article/abs/pii/S0925838819320602 (Accessed: 25 May 2023).
31. Rakhmonov, J.U., Weiss, D. and Dunand, D.C. (2022) *Comparing evolution of precipitates and strength upon aging of cast and laser-remelted al-8ce-0.2sc-0.1zr (wt.%), Materials science & engineering. A, Structural materials: properties, microstructure and processing*. Available at: https://www.ncbi.nlm.nih.gov/pmc/articles/PMC9683509/ (Accessed: 25 May 2023).
32. *Aging temperature* (no date) *Aging Temperature - an overview | ScienceDirect Topics*. Available at: https://www.sciencedirect.com/topics/engineering/aging-temperature (Accessed: 25 May 2023).

APPENDIX 1

Actual data of mixing ratio of alloys

Composition	Al 100% wt.	Al 20% wt.	Mg 100% wt.	Al 2% wt. Sc	Al 2% wt. Zr
Al-15Ce	525	1580	-	-	-
Al-15Ce-0.75Mg	485	1500	15	-	-
Al-15Ce-0.75Mg-0.2Sc-0.2Zr	212	1600	16	238	505

APPENDIX 2

Actual data of stress versus strain curves

1. Representative of stress versus strain curves for Al-15Ce alloy with aging at 150 °C

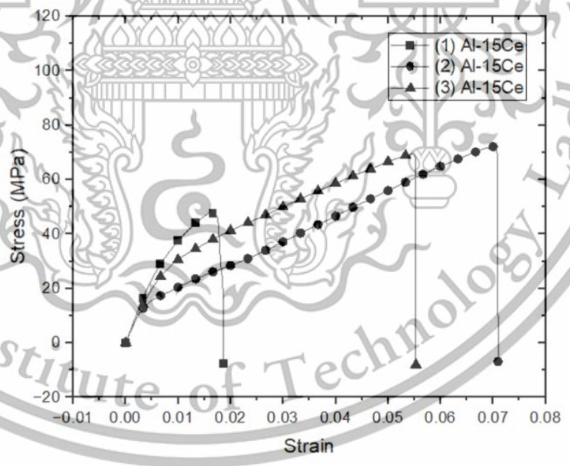

2. Representative of stress versus strain curves for Al-15Ce-0.75Mg alloy with aging at 150 °C

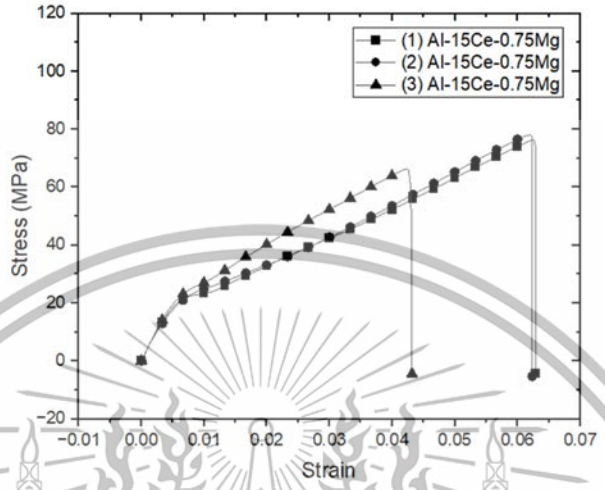

3. Representative of stress versus strain curves for Al-15Ce-0.75Mg-0.2Sc-0.2Zr alloy with aging at 150 °C

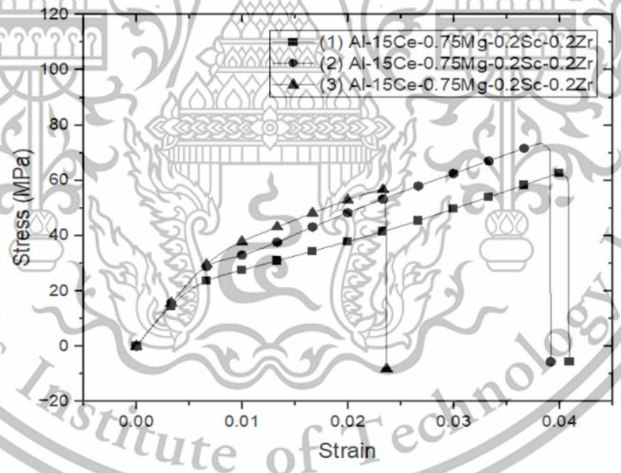

4. Representative of stress versus strain curves for Al-15Ce alloy with aging at 350 °C

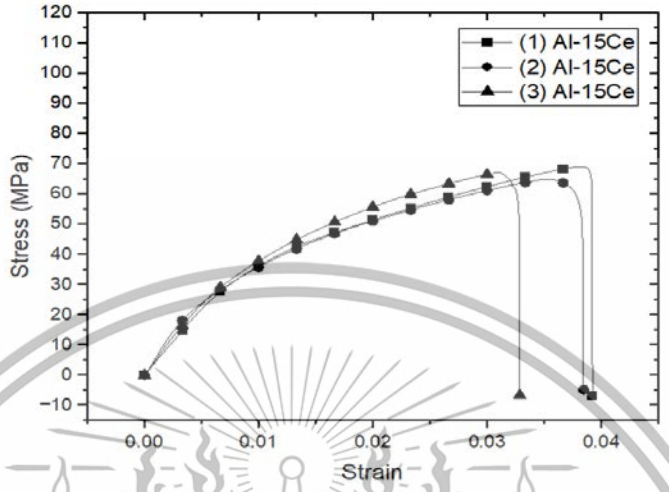

5. Representative of stress versus strain curves for Al-15Ce-0.75Mg alloy with aging at 350 °C

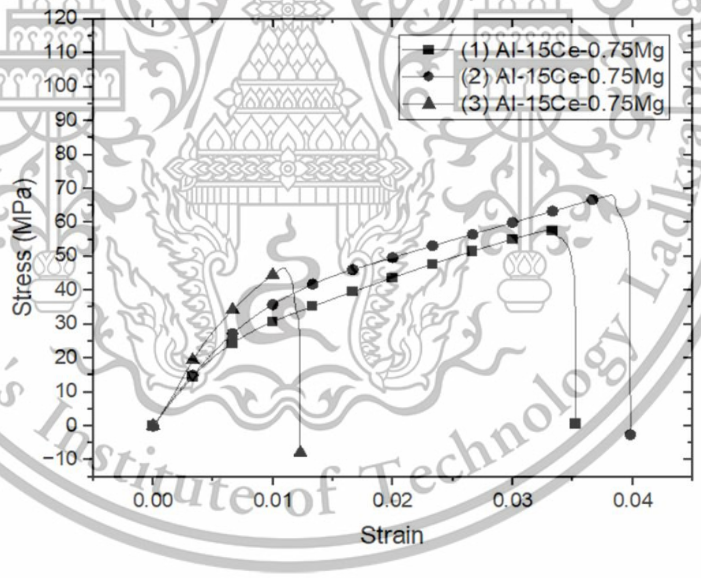

6. Representative of stress versus strain curves for Al-15Ce-0.75Mg-0.2Sc-0.2Zr alloy with aging at 350 °C